CHAPTER 5 : Gases

D. Yi, B. Chaudret, Aikaterini Soulantika

XX Gases

D. Yi[a], B. Chaudret[a] and K. Soulantica[a*]

[a] LPCNO, Université de Toulouse, CNRS, INSA, UPS, 135 avenue de Rangueil, 31077 Toulouse, France.

*corresponding email address: ksoulant@insa-toulouse.fr

ABSTRACT

Dihydrogen and carbon monoxide have been used for many years for the reduction of metals from their ores. These are the two gaseous reducing agents of choice for the synthesis of metal nanoparticles starting from molecular precursors. Their drawbacks (flammability and/or toxicity, use of high pressures) are counterbalanced by an easy removal of the unreacted agents after reaction, and by the fact that they leave no or few residues after use. Apart from acting as reducing agents, they can act as shape directing agents and surface-active species, which influences their structural features and their physical and chemical properties. Last but not least, since during the nanoparticle formation they are present in a large excess, they can be involved in homogenous or heterogeneous catalytic reactions that take place on soluble metal compounds (precursors, intermediate species) or on the surface of the nascent nanoparticles, respectively. These catalytic reactions may influence the nanoparticle formation process and nanoparticle properties.

1 Introduction

Gases, and in the first-place hydrogen, have long been used for the production of reduced metals in a finely divided form. Gas reagents are characterized by an easy diffusion in solids and solutions, despite the low solubility of *e.g.* hydrogen in many solvents. When employed as reducing agents for the formation of nanoparticles (NPs), and depending on the precursor, they leave behind little or no residues and the excess reducing agent is easily separated by gas release. The reducing agent concentration is also easily controlled by the pressure applied, which in turn controls the kinetics of reduction of the precursors. The main drawbacks are associated to flammability and/or toxicity issues and to the use of high pressures. Nevertheless, for many metals, several routinely used non-gaseous reducing agents can also be toxic and/or flammable. In the same context, reduction by gaseous reagents can also be carried out at low, even atmospheric pressure, which reduces the risks associated to high pressure. For comparison sake, a champagne bottle is pressurized at 5-6, up to 8 bars. Although several other reducing gasses exist (NH_3, PH_3, …..), their use in nanoparticle synthesis is practically non-existent. The reducing gases used in the synthesis of metal nanoparticles and discussed here are dihydrogen and carbon monoxide.

The formation of even the simplest colloidal nanocrystal is a complex process in which molecular and surface chemistry operate simultaneously and it is well documented that nanocrystal morphology depends both on thermodynamic and kinetic factors that operate during nanoparticle formation processes.[1] Indeed, at the molecular level, the reducing agents control the rate at which metal atoms are produced from a precursor. Consequently, H_2 or CO pressure may affect the nucleation and growth kinetics by controlling the rate at which “active monomers”

are: i) liberated from the precursor, and ii) deposited on the growing nanocrystals. In this respect, H_2 and CO being mild reducing agents enable a fine control of the reduction rate either by modulating the gas pressure or by playing with the temperature. Additional effects can be expected for H_2 and CO since it is known that small molecules, including gaseous molecules can modify the surface free energy (thermodynamic effect), or impact metal atom diffusion (kinetic effect) on the nanocrystal facets.[2] Thus, they can act as stabilizers themselves, by selectively passivating certain facets of the nascent crystals, or they can even facilitate elimination of other passivating species during growth. The reducing agents may not only reduce the metal center but also the ligands (either native or added) and even the solvent in which the reaction takes place, which can affect the system in disparate ways. Indeed, metals either in their molecular form or as solids can behave as catalysts. The reactions under H_2 or CO can result in hydrogenation or carbonylation reactions that are not desired or not anticipated in the first place.

The purpose of this chapter is not to give a comprehensive list of all the cases in which gas reductants have been employed in the synthesis of metal NPs. We will instead focus on cases where employing gas reducing agents “makes a difference”, that is, examples in which H_2 and CO present advantages or drawbacks and cases in which gas reducing agents have been identified as decisive for the development of interesting features or properties for the resulting metal NPs. Among them a great part is devoted to representative cases in which effects of the reducing gas on the nanoparticle morphology are reported. While the interplay among different factors does not always allow to affirm the role tentatively attributed to the reducing agent, in some cases, specific studies have demonstrated that indeed the gas reducing agent is important in determining nanoparticle morphology either through kinetic or

thermodynamic control of the nanoparticle formation. In this respect, we will present some examples of formation of nanoparticles by reduction or decomposition of molecular precursors using hydrogen. Pure inorganic salts will be treated first. Organometallic and metal-organic complexes will be treated simultaneously in this chapter since the difference is sometimes shallow between these two types of species. We will then describe the formation of NPs by interaction with CO leading either to reduction of the complex or native ligand substitution followed by metal growth.

2. Hydrogen

Hydrogen can be employed as a reducing agent for a large variety of metals. Indeed, it has been used for many years at an industrial scale for the production of ultrapure fine metal powders from their oxides, chlorides, sulphides, sulphates etc in high yields (>99%).[3] Nowadays, there is a renewed interest for hydrogen in the field of metallurgy where it is shown that hydrogen coming from renewable energies may be the future of this industry, given the enormous carbon footprint of the present metallurgical processes. In conventional steelmaking processes, CO_2 gas is produced when iron ore is reduced with CO. H_2 reduction produces H_2O instead of CO_2, thus, this method can be regarded as more environmentally friendly.[4]

H_2 is a reducing agent of intermediate strength,[5] *i.e.* stronger than polyols and milder than sodium borohydride. The reduction of a metal by H_2 can be represented by equation (1).

$$2M^{n+} + nH_2 \rightarrow 2M^0 + 2nH^+ \quad (1)$$

The above equation can be shown as two half cells

$$M^n + ne \rightarrow M^0 \quad (2)$$

$H_2 \rightarrow 2H^+ + 2e$ (3)

The reduction is thermodynamically feasible when ΔG (ΔG_{H2} - ΔG_M) is lower than zero. Since ΔG is related to the reduction potential (E), E_{H2} should be larger than E_M for the reduction to take place ($\Delta G - nFE_{cell}$). E_{H2} depends on the pH and E_M on the metal (oxidation state, coordination sphere, complex stability or lability), therefore, under appropriate conditions, it is possible to reduce even easily oxidizable metals with hydrogen. Nowadays, hydrogen constitutes an ideal reducing agent, routinely used both in industry and in academic research for the reduction of nanoparticles of heterogeneous catalysts after their immobilization on a support and calcination. This use is outside the scope of the present chapter. Here we will discuss the formation of colloidal metal nanoparticles in solution, starting from molecular precursors.

Hydrogen has been employed by the pioneers of colloidal chemistry who used it for the production of platinum metal nanocatalysts. Friedrich F. Nord has described this methodology to prepare platinum metal colloids (Pd, Pt, Rh, Ir) used as catalysts for the hydrogenation of various substrates.[6-9] The advantage was the direct formation of colloidal catalysts by reduction of the metal salt in the reaction mixture containing the substrates to be catalytically hydrogenated. Additionally, no residues that could contaminate the surface of metal nanoparticles were left behind after its use. Since then, a plethora of metal NPs have been prepared by using H_2 to reduce all types of compounds - metal salts, metal-organic and organometallic complexes.

While many theories exist about the formation mechanism of nanoparticles, a great majority of the reports dealing with the synthesis of NPs do not focus on details regarding the reduction mechanism at the molecular level. Nevertheless, reducing a molecular metal species by hydrogen implies an interaction of the gas molecules with the metal compound under consideration. It is thus logic to assume that

oxidative addition and reductive elimination, which are well-known processes in molecular chemistry, are operative during nanoparticle synthesis involving H_2 reduction. The formation of classical metal hydrides is well documented[10] for almost all transition metals. It is therefore expected that hydrides are formed also in the first steps of nanoparticle formation during hydrogen reduction of metal precursors. Subsequently, a series of reactions (reductive eliminations, proton transfers) involving removal and possible transformation of native ligands can produce zero-valent unstable metal species. According to the LaMer classical nucleation theory,[11] clustering of these species could form the first stable solid entities during the nucleation step and the resulting seeds would grow during the growth step. As soon as the solid phase is formed, the interaction of the metal surface comes also into play.[12] Many metals are efficient hydrogenation catalysts and as soon as the solid phase appears, autocatalytic reductions can proceed on the metal surface in a process involving adsorption and dissociation of H_2. Indeed, Finke and Watzky have proposed a two-step mechanism for the growth of metal nanoparticles, where a slow continuous nucleation (A $\rightarrow$ B, rate constant k_1) is followed by fast autocatalytic surface growth (A + B $\rightarrow$ 2B, rate constant k_2).[13,14] This mechanism was based on monitoring the kinetics of the nanoparticle formation through the cyclohexene hydrogenation as a “reporter” reaction (Scheme 1).

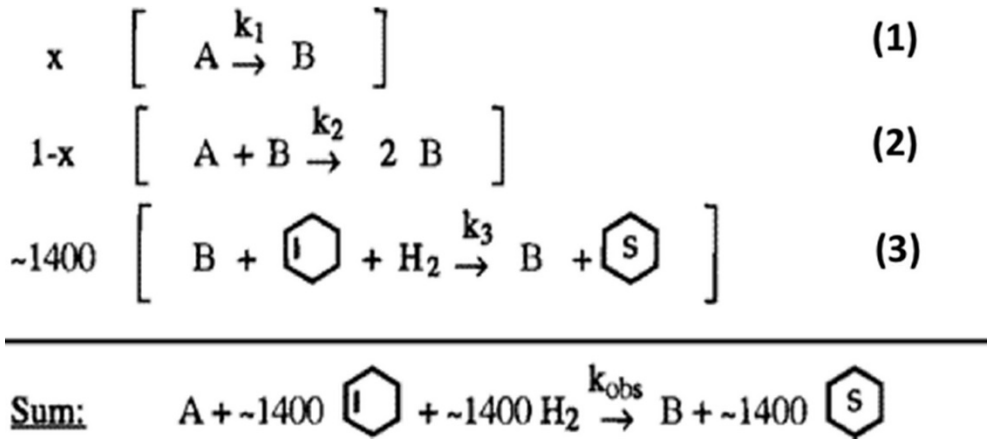

Scheme (1). Generalized two-step formation mechanism and the corresponding rate constants k_1 and k_2. Step (1) represents the nucleation; A corresponds to the organometallic precursor. Step (2) corresponds to the growth; B is a catalytically active atom on the surface of the metal. The reaction is monitored by the fast cyclohexene "reporter reaction" (3). **Reproduced from Ref. 14 with permission from ACS, Copyright 1997.**

This generalized mechanism was proposed in the mid-nineties. In the original paper Finke *et al.* showed that the complex $[(Bu_4N)_5Na_3[(COD)Ir.P_2W_{15}Nb_3O_{62}]$ associating an organometallic iridium moiety to an hetero polyanion could be reduced under mild conditions by H_2 (2.7 atm) at room temperature affording polyanion decorated Ir NPs.[13] Two sizes were obtained: 2 nm when the hydrogenation was carried out in the presence of excess cyclohexene, as part of a catalytic test, and 3 nm when the reaction was carried out in the absence of excess olefins. Interestingly, the authors claim the absence of hydrides at the surface of their catalyst. This and related systems were extensively studied by Finke over the years. The Finke−Watzky mechanism, which involves a slow nucleation and an autocatalytic growth (*i.e.* the decomposition of the precursor over the growing metal surface), was initially based

on thorough kinetic studies on Ir, but it is proposed to be operational in a more general frame, for transition metal nanoclusters formed under H_2 and related reducing agents.[14] This system was used in different hydrogenation reactions, including for example a very active system for acetone reduction.[15] It was also extended to the preparation of stable rhodium nanoparticles of *ca.* 4 nm and to their use for the hydrogenation of cyclohexene.[16]

2.1. Metal salts

Metal salts have been mainly used as precursors in syntheses performed in polar media, including ionic liquids.[17] Alternatively, they have been used in mixtures of polar/nonpolar solvents in the presence of a phase transfer agents (*i.e.* long chain ammonium halides). In classical inorganic salts the metal centers are more electron deficient than in metal-organic and organometallic compounds. H_2 has been used mainly with noble metal salts. Classical salts of low reduction potential metals are not used as precursors with H_2 under the usual conditions employed in wet-chemistry NPs synthesis. It is noteworthy that H_2 is not used to prepare NPs of one of the most easily reducible metals, Au. This is presumably due to the easy reduction of Au(III) salts that are the most popular salt precursors for Au NPs, using non-gaseous reductants. On the other hand, the difficult oxidative addition of H_2 to produce hydride intermediates does not favor reduction of Au(I) precursors by H_2. In fact, pathways to Au-H formation remain elusive, except under some extreme conditions.[18]

Metal salts of Pd, Pt,[6] Rh[7,8] Ir,[9] have been extensively employed for many years for the synthesis of hydrogenation nanocatalysts. The reductions were performed in water in the presence of polyvinyl alcohol and they were efficient under atmospheric

H_2 pressure and room temperature, provided that NaOH was added in order to convert the salts to the easily reducible hydroxides. Based on these results and by adaptation of the same method, tetrahedral and cubic nanocrystals were obtained from K_2PtCl_4 and sodium polyacrylate as a stabilizing agent by El Sayed *et al*.[19] This was an important progress in the synthesis of shape-controlled Pt nanocrystals, despite the fact that in all the studied cases, a mixture of tetrahedral and cubic NPs was present with ratios of each morphology depending on the Pt/capping agent ratio. Nanocrystal shape is among the characteristics that influence nanoparticle physical and chemical properties, to the point that some applications critically depend on it.[20-23] Later, it was concluded that a competition between the reduction and the capping processes modulates the relative deposition rates on the {100} and {111} facets, and therefore the shape of the nanocrystals[24] which is pivotal for their catalytic properties in hydrogenation reactions.[22,25]

Indeed, despite the fact that shape-controlled NPs are obtained in numerous syntheses with H_2,[19,25] H_2 is not routinely considered among the parameters that could influence nanocrystal shape. Below, we present some non-exhaustive cases in which H_2 has been identified as an additional factor that could be involved in the shape control of metal nanocrystals.

Teranishi *et al.* reduced H_2PtCl_6 in the presence of various amounts of sodium polyacrylate and poly(N-vinyl-2-pyrrolidone) (PVP). The dominant shape of Pt NPs was controlled by changing the reduction rate of Pt(IV) ions through two different reducing agents: methanol and H_2.[26] A slow reduction by dihydrogen was proposed to form tetrahedral nuclei initially, while a fast reduction by methanol produced truncated octahedral nuclei. The final Pt NPs preserve the shape of the Pt nuclei at a

high polymer concentration, whereas at a low polymer concentration, the Pt NP shape evolves from tetrahedron to truncated octahedron and finally to cubic.

Fu *et al.* have compared the reduction of three precursors K_2PtCl_4, K_2PtCl_6 and $K_2[Pt(C_2O_4)_2]$.[27] The slower reduction rate of $K_2[Pt(C_2O_4)_2]$ was identified as a decisive parameter for the production of a higher shape selectivity to nanocubes (more than 90%) as compared to the other two precursors.

In another work that illustrates the possible importance of H_2 even when different reducing agents are employed, Somorjai *et al.* have pointed out that the molecular H_2 produced upon $NaBH_4$ reaction with H_2O was the real responsible for the shape control of Pt nanocrystals produced from K_2PtCl_4 and tetradecyltrimethylammonium bromide as a surface stabilizer.[28] Interestingly, *in situ* H_2 gas generation from $NaBH_4$ has been theoretically and experimentally identified by Petit *et al*. as an important parameter for the formation of Pt nanocubes from H_2PtCl_6 thanks to the preferential interaction of H with the {100} facets.[29,30] While H stabilizes selected Pt facets, only ill-shaped Pd nanoparticles were prepared by the same method from H_2PdCl_4. In that case, it was suggested that H_2 induced the formation of the amorphous PdH_x phase by dissociation of H_2 on the metal surface and diffusion of atomic H in the crystal lattice.[29]

Metal salts have also been reduced under H_2 in non-polar solvents, albeit, in the presence of long chain organic stabilizers, mainly amines, that allowed precursor solubilization by formation of different precursor/s, even if this is not always discussed. This method has given access to more complex shapes. For example, Lacroix *et al.*, using H_2PtCl_6 in pure oleylamine under an H_2 atmosphere, synthesized cubic dendrites, planar tripods, and fivefold stars at 150 °C. The control of experimental parameters such as Pt concentration (Figure 1), reaction

temperature, and H_2 pressure, allowed manipulating the reaction kinetics, and through this, the nature of seeds which led to the different morphologies. Noticeably, oleylamine, used as solvent and as a stabilizer, was reduced to octadecylamine during the NPs synthesis due to catalytic hydrogenation by Pt.[31]

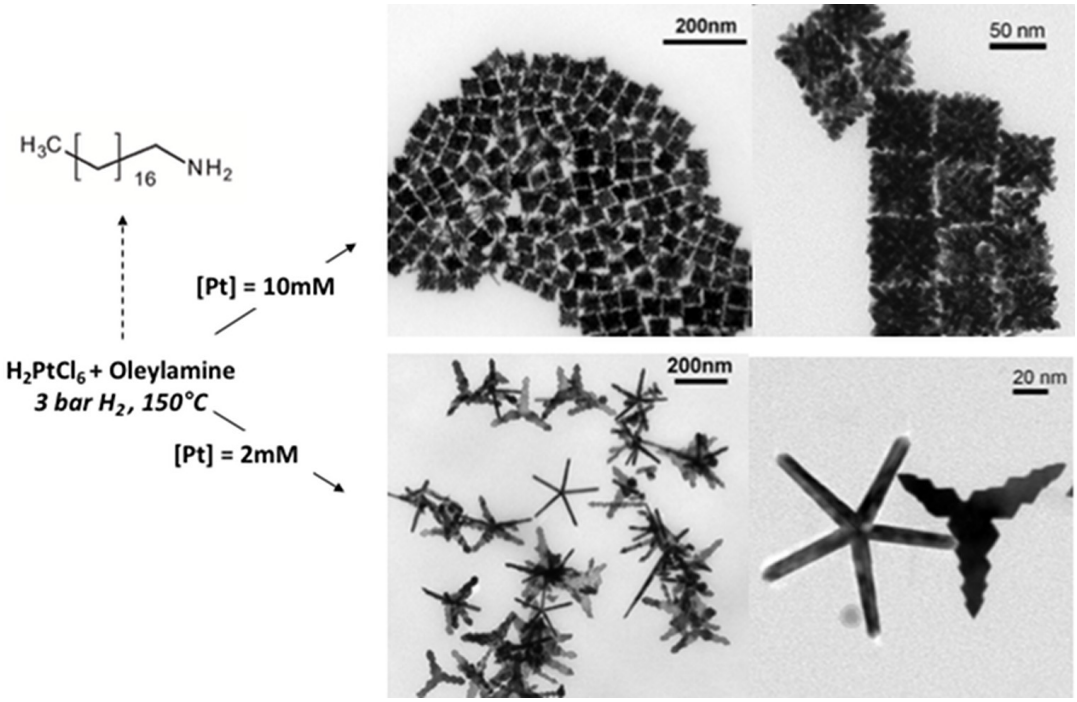

Figure 1. Platinum nano-objects obtained by reduction of H_2PtCl_6 at 150 °C under H_2 (3 bar) employing different precursor concentrations.

In another work, $PtCl_2$ which can be reduced more easily than H_2PtCl_6, has been used in toluene in the presence of an excess of octadecylamine.[32] Pt concave cubes exposing {110} crystallographic facets have been thus synthesized at an impressively low temperature (20 °C). The formation process can be described by a subtle balance between Pt atom production and deposition on the vertices of cubic seeds and diffusion of these atoms to more stable locations on the seed. Several conditions have to be fulfilled, including the use of low temperature, of a sufficient amount of the long chain amine, the use of $PtCl_2$ which produces easily reducible

species upon reaction with the amine and the use of H_2 as a mild reducing agent that can reduce the Pt reservoir at "just the right rate" to allow its diffusion along the edges, a prerequisite for the formation of the cubes enclosed by {110} facets. Increasing the temperature increases the rate of both "monomer" production and diffusion of the Pt atoms, however, "monomer" production seems to be favored over diffusion, since at 60 °C, octopods are obtained due to the fast deposition of Pt on the vertices of the cubic seeds (Figure 2).

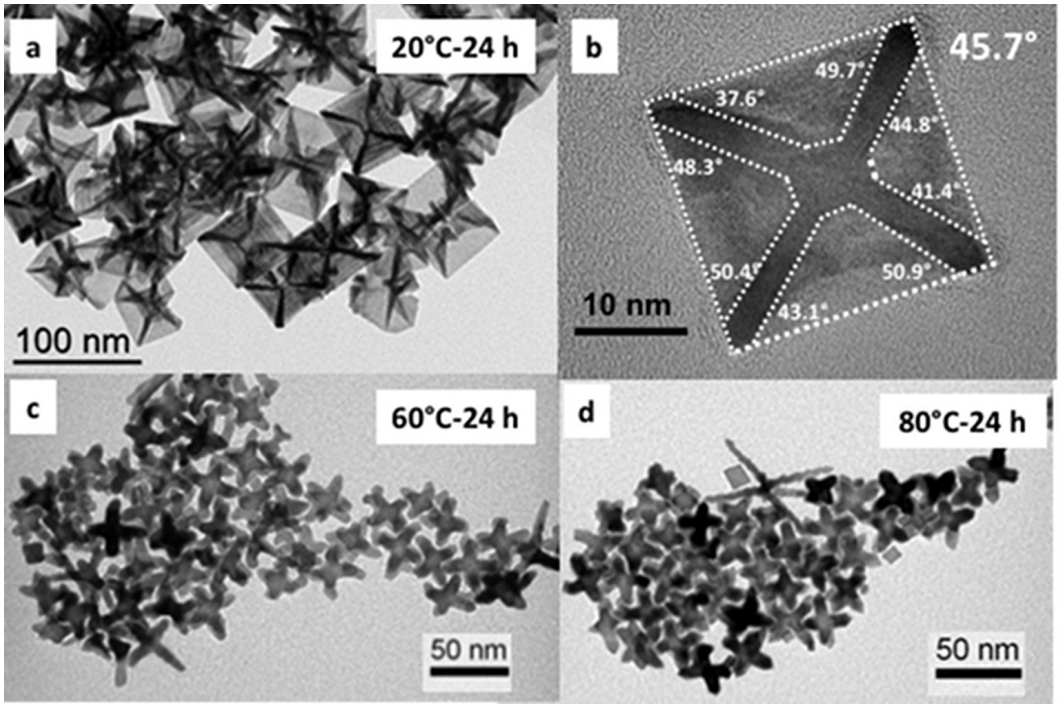

Figure 2. Platinum nano-objects obtained by reduction of $PtCl_2$ under H_2 (3 bar) at different temperatures (a) concave nanocubes exposing {110} facets, (b) HRTEM image of an individual Pt nanocube with the measured dihedral angles; the mean angle of 46° indicates that the exposed facets are of the {110} type.

The octadecylamine used as a stabilizer in large excess can also act as reducing agent, but in the absence of H_2, no concave nanocubes were obtained. In cases where more than one species are present in the reaction medium, reduction may result from more than one source. This is true also for the exact role of other species that can be formed in solution from the starting materials ($PtCl_2$ and octadecylamine, in the above-mentioned example). In addition, when in excess, the amine should trap the HCl formed during the reduction as ammonium chloride. In fact, halides present in many salt precursors and ammonium halide stabilizers added from the beginning or formed during the reaction, are among the species that can strongly adsorb on nanoparticle surfaces in a selective manner depending on the crystallographic orientation of the facets.[33]

2.2. Organometallic and metal-organic compounds

Organometallic compounds involve at least one ligand linked to the metal center through M-C bonds whereas metal-organic complexes contain ligands that are linked through heteroatoms (P, N, O, S, Cl, etc.). Such coordination compounds that do not contain M-C bonds like metal acetylacetonates, carboxylates etc., are the most widely used precursors for metal NPs. For colloidal metal nanoparticle synthesis, H_2 is an ideal reducing agent when the reaction has to be performed in organic solvents, in which other reducing agents cannot be used due to solubility issues. This is the case for almost all organometallic compounds and a great number of coordination compounds for which solubility or chemical stability issues do not allow the use of water-soluble reducing agents.

Reduction of such compounds in the presence of a variety of stabilizing agents and under diverse reaction conditions has allowed a fine control over size, shape,

chemical composition and specific configuration of multicomponent nanostructures (random alloys, intermetallics, core@shell, Janus, etc.). The ligands present on the starting precursors (native ligands) can be displaced completely or partially by the added stabilizing agents. It is therefore important to keep in mind that most of the times, the native ligands stay in solution and are part of the parameters that can affect the reaction outcome. The rich coordination chemistry and its importance in the formation and the properties of metal NPs is outside the scope of this chapter and has been reviewed elsewhere,[34,35,36] but it is worth noting that added stabilizers provide protection against coalescence and, depending on their nature and concentration, they can control nanoparticle size and shape though surface passivation during growth. Added stabilizing ligands may react with the precursors, to transform them into new molecular species acting as metal reservoir. This in turn will affect the course of the reaction (nucleation and growth steps) and its outcome. Therefore, the “real” precursors arise from reactions between the stabilizing agents and the initially introduced molecular metal complex. The different ligands (native or added) present in solution may also participate to equilibria that take place both among the molecular species involved in the reaction process and on the surface of NPs. Finally, ligands, native or added, can be transformed during the whole process of nanoparticle formation. For instance, olefinic bonds can be hydrogenated (*e.g.* cyclooctadiene hydrogenation to cyclooctane, oleyl amine to octadecylamine, partial or complete hydrogenation of aryl substituents of phosphine), native ligands can react with incoming stabilizing agents (*e.g*. incoming carboxylic acids reaction with native silylamide ligands, formation of ammonium salts from amine stabilizing agents and native halides), carboxylates can be decarboxylated, etc.

2.2.1. Organometallic compounds

Organometallic compounds with metal centers in various formal oxidation states have been employed as precursors for the synthesis of a large variety of mono- and bi-metallic NPs through decomposition by hydrogen that may, or not, involve reduction of the metal centre.[34,37-39]

The use of organometallic compounds, lacking in their coordination sphere any ligand that could stabilize efficiently the final nanoparticle surface, constitutes an important knob of controlling the chemical and physical properties by addition of appropriate ligands. This is the case of organometallic complexes containing a metal center, in zero or low formal oxidation state, coordinated exclusively to hydrocarbon ligands through metal–carbon bonds (sigma bonds, pi bonds or a combination of both). Some non-exhaustive examples of metal NPs that have been prepared by this class of organometallic precursors by reaction with H_2 include: Ru from [Ru(COD)(COT)]; (COD = 1, 5 cyclooctadiene, COT = 1,3,5 cyclooctatriene),[40] Pt from $[Pt(Me)_2(COD)]$,[41] and $[Pt(dba)_x]$; (dba = dibenzylidene-acetone),[42] Pd from $[Pd_2(dba)_3]$,[43] Rh from $[Rh(allyl)_3]$,[44] Cu from $[Cu(mesityl)]_5$,[45] Ni from $[Ni(COD)_2]$,[46] Co from [Co(COE)(COD)] (COE = η^3-C_8H_{13}),[47] Re from $[Re_2(allyl)_4]$,[48] Al from $[(AlCp^*)_4]$ (Cp*: penta-methylcyclopentadienyl),[49] or Zn from $[Zn(\eta^1Cp^*)(\eta^5Cp^*)]$.[50] During nanoparticle formation, depending on the oxidation state of the metal and on the ligand type, hydrogen may displace the native ligands with or without reducing them (metal in zero oxidation state), or reduce both metal and native ligands. As a result of the treatment with H_2, “naked” metal atoms and hydrocarbons with no or very low stabilizing ability are produced. The hydrides present on the metal surface cannot stabilize the NP which leads to aggregation of the resulting “naked” metallic atoms and finally in the formation of bulk metal. Therefore, this type of precursors

cannot be employed without the presence of stabilizing agents, which are introduced in the reaction medium before the reduction starts. Thus, nanoparticle stabilization is achieved by a large variety of stabilizing agents,[37, 51-56] which are added in the reaction mixture during synthesis (amines, phosphines, acids, N-heterocyclic carbenes) and even by certain coordinating solvents (*e.g.* THF (tetrahydrofuran), alcohols).[51,57] The possibility that some added stabilizing ligands react with hydrogen, particularly when the reactions are performed at relatively high temperatures,[43,44,53,58-60] has to be considered.

Below we present some examples that highlight the above-mentioned effects that have to be taken into account when reducing organometallic compounds with H_2. Perhaps the most representative example of organometallic precursors, is the ruthenium(0) complex [Ru(COD)(COT)] that has been used for the formation of pure Ru and bimetallic Ru containing NPs.[34] As outlined in Scheme 2, upon [Ru(COD)(COT)] treatment with dihydrogen at room temperature, hydrogenation of the olefinic bonds of the COD and COT ligands produces cyclooctane and “naked” Ru atoms, which subsequently form NPs that cannot be stabilized by the produced cyclooctane.

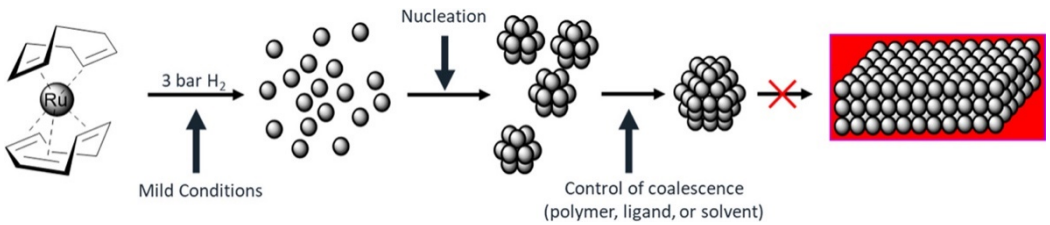

Scheme 2. Outline of the decomposition under H_2 of Ru(COD)(COT). ***Reproduced from Ref.*** *50* ***with permission from ACS, Copyright 2018.***

Compared to other metal NPs, the surface state of Ru NPs has been extensively studied due to the fact that in addition to the classical nanoparticle characterization techniques, liquid- and solid-state NMR studies are particularly well-adapted for this metal, thanks to the absence of magnetic perturbations (Knight shift). The nature and concentration of ligand influence the size and the shape of the NPs.[51,53] It is worth mentioning that, in the presence of amine[61] or carboxylate ligands,[62] mobile surface hydrides are present on the surface of the as obtained Ru NPs. They can exchange with H_2 or D_2 in the gas-phase and even perform H-D exchange reactions on the aliphatic chains of the ancillary ligands.

Surface hydrides are active species involved in a number of heterogeneous catalytic reactions. Their presence on Ru NPs has been detected and quantified by titration with D_2 and with olefins.[61,63] Analysis by gas chromatography has demonstrated the presence of 1.2 and 1.5 H per surface Ru atom, depending upon the system. The observation and location of these hydrides was more challenging, in particular the question of their presence inside the particles or on their surface. For this purpose, the hydrides were exchanged with deuterium and the particles were characterized by static solid state ^{2}D NMR. Thanks to the quadrupolar splitting, which is related to the degree of anisotropy experienced by a quadrupolar nucleus, and the use of model mononuclear compounds to determine the splitting expected for Ru-D Ru-D_2 bonds and clusters containing a μ^2-, μ^3- or μ^6- bridging deuteride, it was possible to observe the presence of surface deuterides and to attribute them a mode of coordination on the particles surface[64,65] (Figure 3).

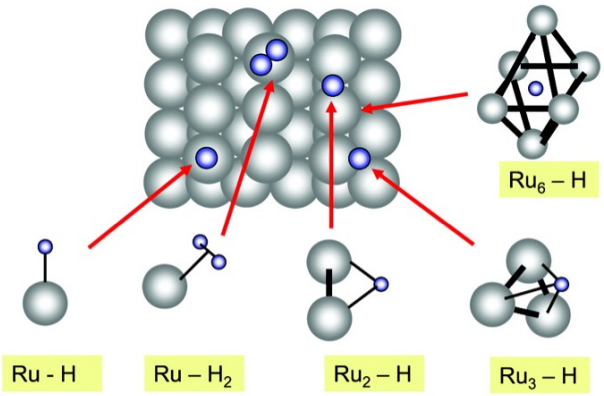

Figure 3. Hydrogen species on Ru metal surfaces. ***Adapted from Ref. 64 with permission from ACS, Copyright 2010.***

Interestingly, this technique evidences the mobility of surface deuterides and the freezing temperature of the deuterium mobility on the particles surface was found dependent upon the stabilizer used. Thus, strong ligands such as diphosphines induce freezing near 273 K whereas the freezing temperature is around 200 K for Ru NPs stabilized by hexadecylamine (HDA)[65] and 25 K for Ru NPs included in a MOF.[66] According to the quadrupolar splitting, all modes of coordination were observed on Ru/HDA, whereas hydrides were exclusively terminal for Ru/MOF. All hydride containing Ru NPs were found to be very active hydrogenation catalysts.[67] N-heterocyclic carbenes have been found to be particularly efficient ligands for ruthenium leading to very stable but reactive nanoparticles accommodating between 1 and 1.5 hydride per Ru surface.[55]

Stabilizing ligands can undergo transformation due to parallel reactions. For instance, it was shown that during the decomposition of [Ru(COD)(COT)] under H_2 in THF in the presence of carboxylic acid ligands, CO was found on the surface of the NPs. This CO arises both from THF decomposition and from carboxylic acid

decarbonylation.[68] The latter occurred at surprisingly low temperature (room temperature). Catalytic decarbonylation of carboxylic acids in the presence of dihydrogen usually occurs at much higher temperatures and pressures, suggesting an unanticipated high reactivity of undercoordinated Ru species that are formed during the decomposition of [Ru(COD)(COT)] in the presence of H_2 and carboxylic acids. Another example is the partial hydrogenation of fullerene ligands catalyzed by Ru NPs prepared from [Ru(COD)(COT)] and fullerene under H_2.[59] Partial or complete catalytic hydrogenation of the aryl rings of phosphine ligands has also been demonstrated through deuteration experiments.[60]

The Ru NPs prepared through the organometallic method are also very active for the selective labelling of organic molecules of interest through C-H activation.[69] This method was extended to the unprecedented simple enantiospecific C-H activation/deuteration of stereogenic centers, located in α-position of a heteroatom of amino acids and peptides through a four-membered dimetallacycle as a novel key intermediate.[70] Ru NPs are also active catalysts for the Sabatier reaction and for Fischer-Tropsch syntheses. In this context, the presence of CO leads to the elimination of surface hydrides and only CO species are adsorbed at the surface of the nanoparticle.[71]

These examples illustrate the multiple role that hydrogen can play, that is, as a reducing agent and as a key surface species available both for stoichiometric as well as for catalytic reactions. This can be advantageously exploited in catalysis, when, either an easy access to the nanoparticle surface is considered as a prerequisite for increased catalyst activity,[51,52] or as shown recently, when the presence of specific ligands on the nanoparticle surface positively impacts not only selectivity but also activity.[72,73] A recent review, and references therein, presents the knowledge

accumulated over the years on the formation, surface chemistry and catalytic properties of Ru NPs obtained by [Ru(COD)(COT)].[51]

Another important advantage of employing H_2 as reducing agent is that it can produce impurity- and oxide-free metallic NPs of easily oxidizable metals. The excellent magnetic properties of metallic magnetic NPs prepared by reduction under hydrogen are due to a surface free from oxides and other contaminating residues that could be present if another reducing agent (CO, $NaBH_4$) was employed. For example, magnetic properties of ultrafine Co NPs prepared by [Co(COE)(COD)] in the presence of PVP as a stabilizing agent, present the same size dependent magnetization values as the ones of NPs of similar size[74] prepared by ultrahigh vacuum techniques. Due to their small size and consequently due to the increased contribution of surface metal atoms to the magnetization value, these NPs exhibit magnetizations that exceed the bulk magnetization value of bulk Co.[75] These results prove that PVP, used as stabilizing agent, does not affect the magnetic properties of the above NPs. However, this is not the case for all stabilizers. Indeed, the electronic density of the nanoparticle surface can be modified by the presence of capping agents, thus altering several chemical and physical properties among which magnetic properties. This effect is illustrated by the work of Osuna *et al*., who have shown that reaction at room temperature of the above-mentioned NPs with CO gives rise to a spectacular drop of their magnetization, due to the presence of CO on their surface.[76] This ligand dependent effect on the magnetic properties has been also observed for Ni NPs prepared by reaction of $[Ni(COD)_2]$ with H_2 and then exposed to CO or MeOH, or alternatively, prepared in the presence of hexadecylamine (HDA) or trioctylphosphineoxide (TOPO).[77] It was shown that among all four stabilizing agents, only HDA preserves the Ni surface magnetization.

Ligands do not affect the nanoparticle properties only through surface effects, as they play multiple roles in nanoparticle synthesis. Ni NPs prepared by reaction of [Ni(COD)$_2$] with H_2 in the presence of high amounts of HDA grow anisotropically.[77] The reduction under H_2 of the [Co(COE)(COD)] precursor in the presence of both long chain amines and long chain acids as stabilizers produced for the first time cobalt nanorods of *hcp* (hexagonal close packed) structure.[78] The combination of high magnetocrystalline anisotropy and the anisotropic growth along the *c* axis of the *hcp* structure of Co make these nano-objects well-adapted for applications for which hard magnetic materials are necessary, such as magnetic recording. The ligands, especially the carboxylates, are beyond any doubt decisive in the anisotropic growth of these nanorods as is the presence of H_2. All other parameters kept identical except the presence of H_2, no Co nanorods/nanowires are obtained by the organometallic method.[78,79] It is likely that H_2 displaces the long-chain amine, which transiently passivates the {0001} facets of *hcp* seeds, thus allowing deposition of Co atoms on these facets and anisotropic growth.[80] A similar ”cleaning” effect of H_2 that facilitates coalescence through temporary amine ligand removal from the surface of NPs has been invoked in the formation of Pt,[4] Ru,[53] and Pd[43] anisotropically shaped NPs.

Therefore, and despite the tedious synthesis of organometallic compounds and their low stability which often requires specific handling precautions, the combination of this class of precursors with H_2 facilitates surface studies. It also offers the opportunity to adapt the NP surface chemistry to meet the prerequisites of technological domains spanning from catalysis to microelectronics, introducing the appropriate stabilizing agent for each application.

When in addition to, or instead of the non-coordinating hydrocarbons the precursor contains ligands that have considerable coordinating ability (halogens, carbonyls, amide, amidinate, carboxylate compounds) their involvement in the stabilization of the NP surface, but also in the NP formation steps has to be considered.

2.2.2. Metal-organic compounds

Metal alkylamides $M(NR_2)_n$ and silylamides $M[N(SiMe_3)_2]_n$ have started to be used relatively recently for the synthesis of metal NPs.[81-83] They share common characteristics with organometallic compounds, containing olefinic ligands in the sense that they are easy to be reduced at low temperature. However, while in the presence of H_2, the olefinic ligands are hydrogenated and cannot act as stabilizers: the amide can be converted to hexamethyldisilazane, which can stabilize small Nps as shown in the work of Margeat *et al*., in which $\{Fe[N(SiMe_3)_2]_2\}_2$ heated under H_2 at 110 °C in toluene gave rise to purely metallic iron NPs that could be isolated.[84] In the presence of mixtures of long chain amines and acids, $\{Fe[N(SiMe_3)_2]_2\}_2$ and $\{Co[N(SiMe_3)_2]_2THF\}$ have been decomposed giving rise to oxide-free shape controlled Fe[81,85] and Co[80,86] NPs as well as Co-Fe dumbbells[87] or FeCo alloys,[88] depending on the reaction conditions. All nanoparticles display excellent magnetic properties thanks to the absence of surface oxides on their surface. When silylamide precursors are used in the presence of amine and acid stabilizers, the formation of Fe and Co carboxylates is of pivotal importance, since thanks to their stability they constitute a metal reservoir that contributes mainly to the slow growth of seeds formed by less stable amine rich species. It must be noted that care has to be taken when mixing $\{Fe[N(SiMe_3)_2]_2\}_2$ and $\{Co[N(SiMe_3)_2]_2THF\}$ with long chain acids, since the formation of metal carboxylates is in competition with the formation of a silyl ester

by reaction of the acid stabilizer with the native ligand. This was demonstrated to have an impressive impact on the size and the morphology of the resulting NPs.[88] Acetates and long chain carboxylates are easily accessible starting materials, however their increased stability toward reduction by H_2 requires higher reaction temperatures than organometallic compounds. Despite the fact that they are rarely used as starting precursors,[89,90] carboxylates are often formed *in situ* due to the use of carboxylic acids as stabilizing agents, starting from precursors of various types. Due to their stability they mainly participate to the growth step of seeds. In this context, under reaction conditions that do not allow reduction of $Co(LA)_2$ (LA= laurate) by H_2, the addition of hexadecylamine allows the formation of cobalt multipods. This could be due to the possibility of heterolytic activation of H_2 through coordination to the Lewis acidic species and deprotonation by the amine.[86]

In a recent work concerning Ni branched nanostructures obtained by $[Ni(CH_3COO)_2]$ in the presence of oleylamine, and combining theoretical and experimental results it was proposed that in the absence of H_2 the growth is controlled mainly by thermodynamics. Thus, the NPs are ill-defined polyhedra enclosed by {111} and {100} facets. Under a 6 bar hydrogen pressure, the obtained octopods result from a seed exposing mainly {100} facets through a three steps growth, which is governed both by kinetics and thermodynamics. At a short time, a kinetically controlled preferential orientation along the <111> direction forms octapods. Upon consumption of the precursors with time, the synthetic process falls into the thermodynamic regime, in which the growth along the <110> direction becomes dominant. Under 14 bar of H_2 pressure, and starting from a seed that exposes mainly {110} facets, the slower Ni surface diffusion rate combined to the faster deposition rate makes the synthetic process fall in the kinetically controlled regime. In this case, the high

surface energy facet of Ni(111) grows more quickly (Figure 4). The influence of the adsorption of the oleylamine ligand and of the solvent (ethanol) on the synthesis process of Ni nanocrystals was found to be negligible according to the corresponding adsorption energies, but the possible influence of carboxylates coming from the precursor $Ni(CH_3COO)_2$ has not been considered.[91] In a subsequent work combining modelling and experiments from the same group, the H_2-induced increase of the reduction rate of the Ni precursor has been also considered. It was proposed that this increase also favored the overgrowth on Ni nuclei toward branched nanostructures.[92]

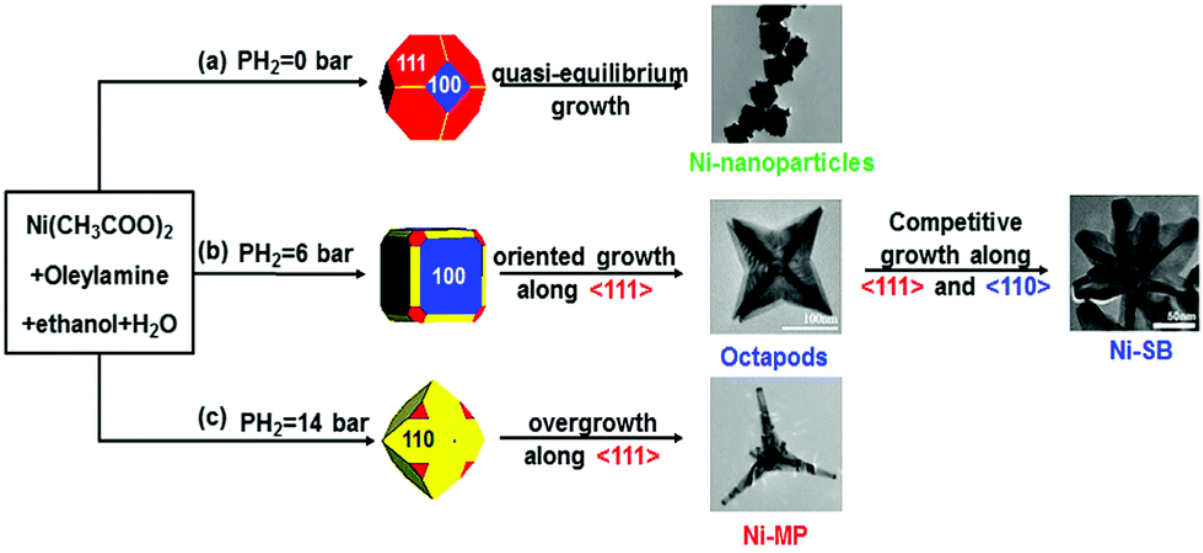

Figure 4. Outline of the H_2 pressure influence on the formation of branched Ni nano-objects. ***Reproduced from ref. 91 with permission from the PCCP Owner Societies Copyright 2017***

The most popular coordination compounds used as precursors for monometallic and bimetallic NPs are metal acetylacetonates. Below we present some examples where H_2 has been identified as a factor that contributed to the shape-controlled synthesis.

In several cases however, its exact role as a structure directing agent remains rather unclear.

In a work of Tilley and co-workers Ni nanocube formation from $[Ni(acac)_2]$ in the presence of hexadecylamine and trioctylphosphine oxide has been tentatively attributed to the thermodynamic stabilization of Ni {100} facets favored by H_2.[93] In another study by the same group, the increase in the H_2 pressure from 1 bar to 3 bar results in a phase transformation of Ni from *fcc* (face centered cubic) to *hcp*, which leads to anisotropic growth of arms on a *fcc* Ni or Au seed,[94] or *hcp* Ni branches on Au *fc*c seeds.[95]

Pt-based NPs of complex shapes are among the most desirable nanostructures especially for electrocatalysis and a great effort is devoted for developing catalysts that optimize Pt atom efficiency.[96] In this context dendritic nanocubes have been obtained when $[Pt(acac)_2]$ was heated at 90 °C in pure oleylamine, under 1 bar hydrogen atmosphere.[97] Interestingly, the oleylamine (solvent and stabilizing agent) was converted to octadecylamine during the formation of the Pt nano-objects. More precisely the whole amount of oleylamine was hydrogenated in 24h. In the absence of H_2, ill-defined nano-objects are obtained. The dendritic nanocubes are similar with some of the nano-objects obtained from Lacroix *et al*. with H_2PtCl_6 in oleylamine under 3 bar H_2 at 150 °C.[31]

Mao *et al.* using $[Pt(acac)_2]$, $[Mo(CO)_6]$, and $[Ni(acac)_2]$ in the presence of oleylamine under 180 °C synthesized PtMoNi ultrathin nanowires.[98] The authors did not succeed in synthesizing the nanowires in the absence of H_2, and they propose that Pt rich nanowires are formed in a first step thanks to hydrogen that functions both as a structure directing agent and as a mild reductant for Pt^{2+}. The Pt surface assists the subsequent reduction of the harder to reduce Ni^{2+}.

In situ hydrogen production resulting from other reductants ($NaBH_4$, hydrazine, polyols) is also probably involved in determining nanocrystal shape. Interestingly, in the formation of Co nanorods by the polyol method, using 1,2 butanediol as a reducing agent, the secondary alcohol function of the polyol was shown to be selectively oxidized to a ketone with the concomitant formation of molecular hydrogen (transfer hydrogenation reaction). It is thus likely that the *in situ* produced H_2 contributes to the Co shape control.[99]

Homoleptic metal carbonyls have been extensively used for the preparation of metal NPs, but rarely employed with H_2 since the metal centers being already reduced, no reducing agent is needed. However, in an example that illustrates the parallel catalytic reactions that can take place with H_2 and CO, Ru nanostars and nanourchins have been prepared by thermolysis of $[Ru_3(CO)_{12}]$ under H_2 in the presence of hexadecylamine and palmitic acid.[58] The gas analysis at the end of the synthesis revealed the presence of methylcyclohexane resulting from the hydrogenation of the toluene solvent, as well as that of linear alkanes, which were most likely formed by the activity of the Ru NPs as a Fischer-Tropsch catalyst.

In conclusion, the examples presented in this part show that apart from reducing the precursors in which the metal center is not in the zero-oxidation state, H_2 can reduce native ligands, stabilizing agents as well as organic substrates and even solvents, either when coordinated to a soluble compound or when chemisorbed on a metal nanoparticle. Last but not least, dihydrogen can be a shape directing agent through modulation of the nucleation and growth steps and facet selective passivation (Scheme 3).

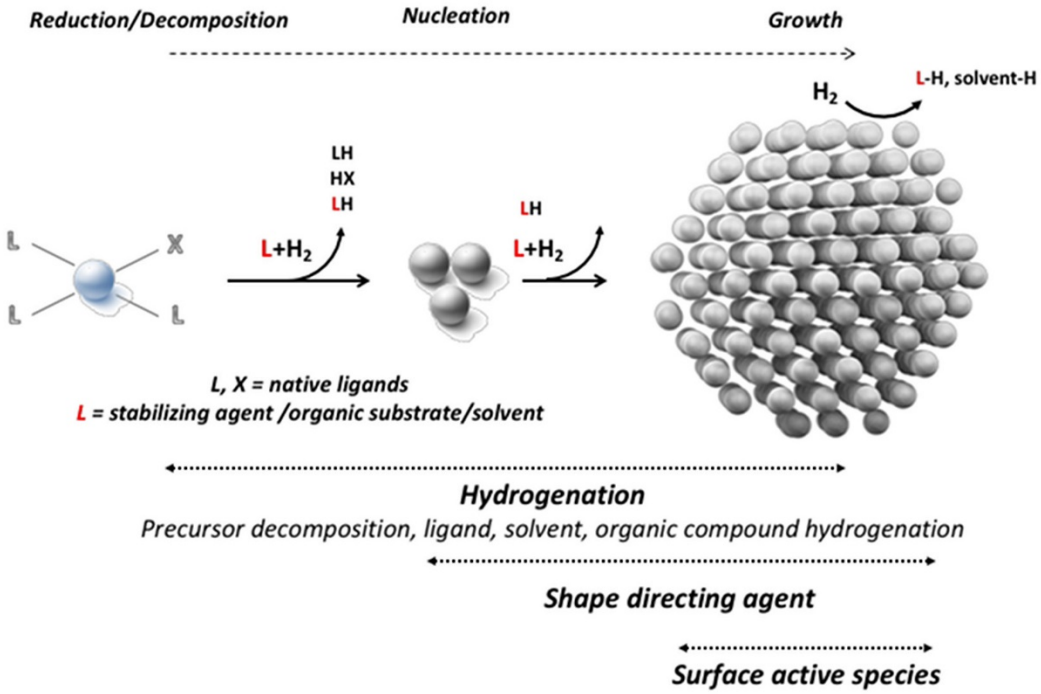

Scheme 3. Different roles of H_2 throughout all the steps of the NPs formation process.

3. Carbon monoxide

The reducing strength of CO is comparable to that of H_2,[100] but it can also form metal NPs without reducing the metal center, as for instance by displacing at room temperature labile ligands from organometallic precursors in which the metal center is in the zero oxidation state. CO has been used in the synthesis of metal and metal alloy NPs, either by direct gas admission, or alternatively, through the decomposition of metal carbonyl complexes. Its usual oxidation product (CO_2) is inert and easily eliminated from the reaction medium. Apart from being a reducing agent, the CO molecule is one of the most important ligands in transition metal chemistry. Thanks to its ability to both donate and accept electrons from transition metals, it plays a prominent role in the design of catalysts used in many carbonylation reactions. CO

612 reacts with metal centers in low oxidation state to form metal carbonyls, whereas
613 interaction with metal centers in high oxidation state needs previous reduction and is
614 weak.[101] In addition, CO can interact strongly with metal surfaces, with chemisorption
615 behavior that differs not only from one metal to another but also from one
616 crystallographic surface to the other for the same metal.[102] Thus, it can behave as
617 strong shape directing agent as illustrated from the numerous examples in the
618 literature where shape control is attributed, at least in part, to CO.[103] Once CO
619 reduction or ligand displacement has formed the first solid entities, additional CO
620 reactions on the metal surface can be operational. Numerous studies on
621 heterogeneous catalysis have demonstrated that, depending on the nature of the
622 metals and the temperature of the reaction, CO chemisorption can be either
623 molecular or dissociative. Transition metals such as Fe, Co, or Ni favor CO
624 dissociation while adsorption on noble transition elements is non-
625 dissociative.[102,104,105] Therefore, depending on the metal and the reaction conditions
626 (temperature, presence of other gases among which H_2) the metal NPs can be very
627 different in nature (reduced metals or metal carbides) or have a very different surface
628 state (CO passivated or not), with important consequences on their physical and
629 chemical properties. Below, we present some non-exhaustive examples, which give
630 an overview of the rich chemistry associated to the use of CO in nanoparticle
631 synthesis.
632
633 **3.1. Ligand displacement without reduction**
634 CO has been extensively used in the synthesis of Pd and Pt metal NPs starting from
635 the zero-valent organometallic precursors ($[Pd_2(dba)_3]$ and $[Pt(dba)_x]$), through
636 displacement of these ligands.[40,106,107] Since NPs are formed at low temperature, the

CO is adsorbed intact on the nanoparticle surface at the end of the reaction. Due to its surface dependent and multimodal adsorption on metal surfaces, it is a particularly useful molecule for probing the surface of metal particles. Stretching vibrations of the C≡O bond appear in the IR spectrum between 2200 and 1700 cm^{-1} and the CO binding mode (atop, bridging, hollow) can be identified by the position of the signals.[40,108] Solid state ^{13}C NMR techniques developed for probing heterogeneous catalyst surfaces[109] have been very successfully applied to the domain of colloidal NPs in studies concerning both surface state and reactivity.[72,107,110-112] On the other hand, CO can persist on the final nanoparticle surface and it may affect their physical,[75,79] and chemical properties. These latter can be severely impacted since CO acts as a poison of active sites in many catalytic reactions.[113]

3.2 Mild reducing agent for reaction monitoring

There are only few examples in the literature of studies that propose reaction pathways where reduction by CO gives rise to metal NPs. The slow reduction kinetics by CO compared to $NaBH_4$, enabled the CO induced synthesis of thiolate protected Au nanoclusters $Au_{25}(cys)_{18}$ (cys = cysteine) to be followed. The clusters were prepared from $HAuCl_4$ and cysteine in aqueous basic solution (pH = 11) at room temperature.[114] CO interaction with the Au(III) metal center is not favored. Despite the fact that cysteine is a milder reducing agent than CO, it can perform the first reduction from Au(III) to a Au(I)-thiolate complex. CO can then perform the second reduction step. The slow reduction by CO allowed monitoring of the $Au_{25}(cys)_{18}$ formation process by UV-Vis and mass spectrometry, and identification of several key intermediates. Increasing the pH enhances the reduction capability of

CO. The authors observed that CO was not present on the surface of the nanoclusters probably due to the catalytic activity of Au nanoclusters in alkaline conditions for CO oxidation to CO_3^{2-}. This CO mediated synthesis has been extended to other $Au_n(SR)_m$, nanoclusters[115] and a review on this method has been published.[116]

3.3 **Homogeneously catalyzed ligand carbonylation**

CO is not only a reducing agent that is converted to inert CO_2 during nanoparticle formation. A multitude of carbonylation reactions can take place in the presence of molecular metal precursors that are acting as catalysts. This is illustrated in a work in which [$Pt(CH_3)_2$(COD)] was reduced by CO at atmospheric pressure in the presence of hexadecylamine (HDA) and oleic acid. CO, rapidly substitutes COD leading to the formation of [cis-$Pt(CH_3)_2$(CO)(HDA)] and [cis-$Pt(CH_3)_2(CO)_2$] which were identified by ^{1}H and ^{13}C NMR. Upon heating at 110 °C under CO, complete decomposition of the molecular Pt compounds occurs, giving rise to Pt(0) NPs stabilized by a mixture of N,N'-bis(hexadecyl)urea and CO ligands as shown by IR and ^{13}C NMR studies. In addition, NMR analysis of the supernatant at the end of the reaction evidenced the formation of a secondary amide identified as N-(hexadecyl)acetamide, CH_3CONHR, and a small amount of N,N'-bis(hexadecyl)urea. These results indicate that HDA carbonylation has taken place.[117] The decomposition outline that is proposed to account for the carbamide formation through [cis-$Pt(CH_3)_2$(CO)(HDA)] is shown in Scheme 4. This work evidences the complexity of the reactions taking place during nanoparticle synthesis.

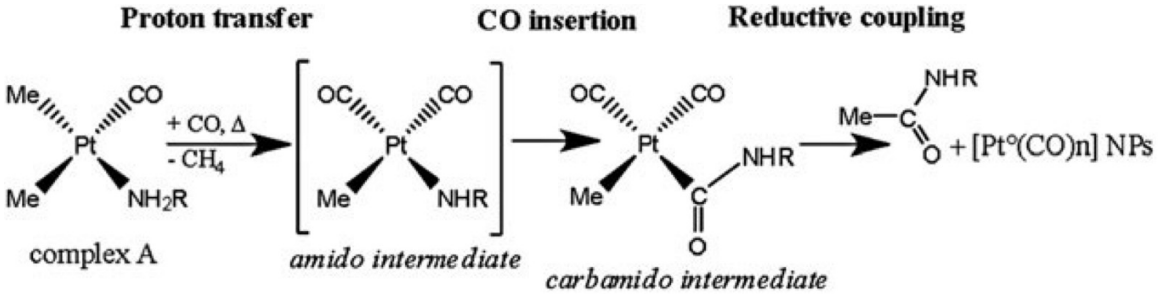

Scheme 4. Outline of the proposed reactions taking place on the Pt center during the formation of Pt nanoparticles. ***Reproduced from ref. 117 with permission from The Royal Society of Chemistry Copyright 2010***

Similar reactivity was demonstrated when Au NPs were obtained from the reduction under CO of $AuCl(NH_2R)$ complexes formed *in situ* from AuCl(THT) (THT = tetrahydothiophene). While H_2 fails to yield size and shape controlled Au NPs under all the conditions employed, the use of long chain amines (dodecylamine or hexadecylamine) as stabilizing agent in THF at 70 °C in the presence of CO (1 bar) leads to stable and well-defined Au NPs of about 7 nm and with a narrow size distribution. Solid-state ^{13}C MAS NMR and liquid state ^{1}H NMR studies demonstrated the presence of a carbamide (RNHCONHR) species resulting from the carbonylation of the amine on the Au NPs. The authors noted that this unexpected reaction has a positive effect on the NP stability.[118]

3.4 CO as shape directing agent

As already mentioned, several physical and chemical properties depend on the nanoparticle shape. A consequence stemming from CO affinity for metal surfaces is that it can act as a shape directing agent by selectively passivating certain nanocrystal facets during growth. The interest in metal nanocrystal synthesis is

largely associated to the optimization of their catalytic properties. Considering that the performances of catalysts are dependent on the type and number of exposed facets, tailoring of metal nanocrystal morphology is currently a very active area of research.[119] Since Pt- and Pd-based catalysts are among the most widely applied in thermal catalysis as well as in electrocatalysis, an intense research activity concerns the control of their shape. Furthermore, CO assisted growth of Pt and Pd shape-controlled NPs has paved the way to the development of this method for their alloys,[2,120-122] as well as for other metals.[103,123] In most of these cases, metal and facet depending adsorption of CO during nanocrystal formation is claimed to be one of the crucial parameters for shape control.

Metal carbonyls such as $Fe(CO)_5$,[124] $Co_2(CO)_8$,[125] and $W(CO)_6$[126] have been demonstrated to play a decisive role in the formation of shape controlled NPs, especially in the case of cubic Pt and shape controlled Pt-based alloys.[127] In some works the possible role of CO from the decomposition of the metal carbonyls has been ignored and the morphology has been attributed to the reducing capability of the zero valent metal of the carbonyl complex, which assisted the reduction of Pt(II) and regulated the nucleation process. However, other works have demonstrated that the presence of CO alone is enough to induce the formation of specific morphologies depending on the nature of the NPs.[128] Compared to metal carbonyls, the use of CO has the advantage that it does not introduce any metal impurities, that could be finally found in the target nanocrystals. Thus, C.B. Murray *et al.*, have reported the rapid formation of monodisperse Pt nanocubes from $[Pt(acac)_2]$ in the presence of oleylamine and oleic acid, Pd spherical nanoparticles from $[Pd(acac)_2]$ in the presence of oleylamine, oleic acid and TOP (trioctylphosphine), and ultrathin Au nanowires from AuCl in the presence of oleylamine, when CO was bubbled through

their solutions in organic media.[128] The absence of CO bands in the IR spectra obtained from the Pt nanocrystals and a control experiment after having evacuated bubbled CO before heating, led the authors to the conclusion that CO was acting as reductant and not as a capping agent, and that the observed shapes were not formed due to the formation of a CO containing precursor. The authors assigned the nano-object shape to the fast reduction kinetics induced by CO.

However, Wu *et al*. correlated the cubic shape of Pt NPs with the preferential binding of CO on {100} facets. Pt nanoparticles prepared from [$Pt(acac)_2$] at 180 °C in the presence of oleylamine and oleic acid under CO adopt a cubic shape. More precisely, it was shown that while both amine and CO were necessary for the formation of cubic nanostructures, the presence of oleic acid was not necessary (Figure 5).[129] Their results were supported by IR analyses, which confirmed the presence of CO and oleylamine on the nanocube surface, and periodic DFT calculations that showed that the Pt(100) surface can be significantly stabilized by the co-adsorption of CO and oleylamine.

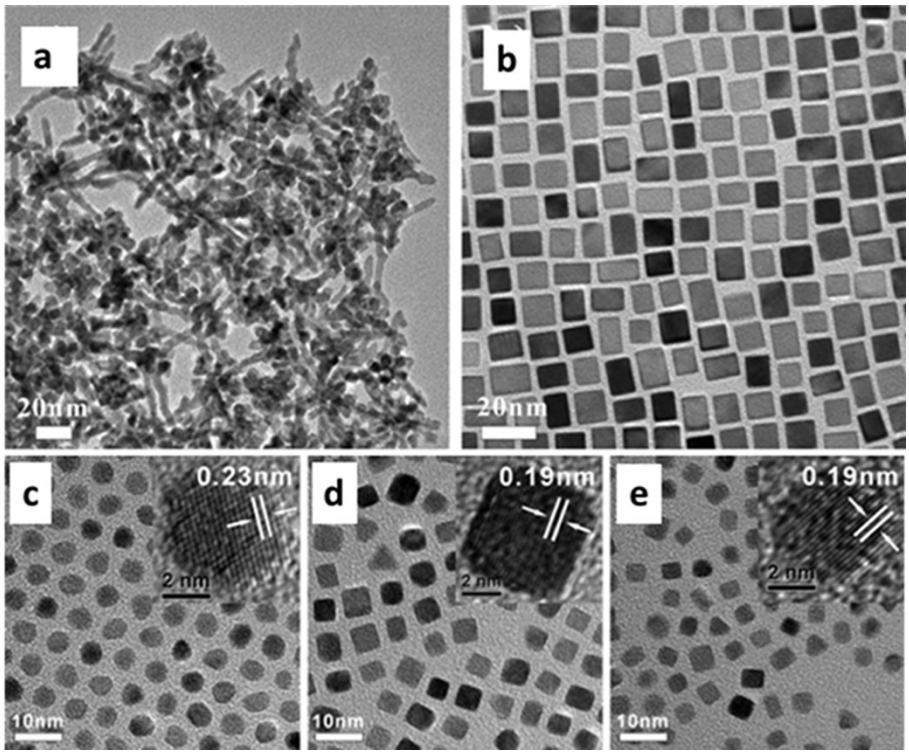

Figure 5. TEM images of (a) Pt nanodendrites synthesized without CO; (b) 10.3 nm Pt nanocubes prepared under CO flow at 180 °C, both using 4 : 1 oleylamine/oleic acid; (c) spherical NPs in pure oleylamine under CO flow; (d) in pure oleylamine under 1 atm CO and (e) under 2 atm CO. The insets are the corresponding HRTEM images. ***Adapted from ref. 129 with permission from The Royal Society of Chemistry Copyright 2011***

In that case oleic acid did not seem to be essential for obtaining the cubic NPs since even in its absence, the cubic shape was obtained by CO and oleylamine. However, very recently, oleic acid was shown to be a decisive actor allowing Pt cubes and bars to be obtained when using the same as above precursor [$Pt(acac)_2$], which was dissolved in oleic acid and heated at 80 °C. The authors propose that this step leads to [$Pt_3(oleate)_6$]. Subsequent increase of the temperature to 120 °C leads to oleic acid catalytic decarbonylation, presumably from [$Pt_3(oleate)_6$], which was proposed as a Pt(II) intermediate. The authors claim that the CO produced by this step acted as a reducing agent to provide Pt(0) atoms, and as a capping agent stabilizing {100} type facets of the nanoparticles.[130] The authors mention the different catalytic reactions likely to take place on the Pt surface.

Under the light of these recent results, one may wonder why decarbonylation of the oleic acid did not take place under the very similar (even harsher) reaction conditions employed in the work of Wu *et al*.[129] Indeed, in that work, there was no indication of CO production. It is therefore likely that other catalytic reactions are favored under those conditions. Several shape-controlled Pt-based alloys with a great variety of metals have been synthesized since the first Pt nanocubes formed through the CO reduction by [$Pt(acac)_2$].[126,127,131]

Wu *et al*. proposed that preferential binding of CO on the {100} facets could also favor addition of metal atoms onto specific facets of Pt alloy nanocrystals, because CO can undergo preferential oxidation to CO_2 on selected surfaces.[127] Nevertheless, based on several works on the synthesis of Pt_3M nanoparticles (M = Fe, Ni, Co), it seems that the presence of CO alone is not enough, and several conditions have to be met (temperature ramp, stabilizing agents, etc.) to guarantee stoichiometry and shape selectivity of the resulting NPs.[126,127,131]

In contrast to what is observed on Pt, CO binds preferentially on Pd{111} facets. As a result, Pd NPs adopt shapes that expose {111} facets such as ultrathin nanoplates and nanosheets. Nowadays, one of the preferred methods for the synthesis of 2D ultrathin NPs of many metals is based on the so-called CO "confined growth" in solution which designates the characteristic limitation of the 2D nano-objects thickness to a few atomic layers, by selective adsorption of the CO on the highly exposed {111} basal facets of the 2D Pd based nano-objects.[132]

In an early work Schlotterbeck *et al*. obtained, "somewhat surprisingly" as they stated, hexagonal platelets with a relatively narrow size distribution through reduction of $[Pd(OAc)_2]$ by CO at room temperature, in toluene solutions of amphiphilic polymers. In comparison, reduction with H_2 or $LiBEt_3H$ afforded spherical palladium NPs. Although an interpretation of this result was not straightforward, the authors note that the reduction is much slower with CO than with the other reducing agents and that unstable Pd(II) carbonyl compounds are intermediate species.[133]

Remita *et al*. synthesized ultrathin hexagonal Pd nanosheets in a water/toluene mixture purged with CO gas[134] from precursors in which Pd was in different formal oxidation states. A 2D morphology was obtained in all cases, except in the case of $[Pd_2(dba)_3]$, which reacted very fast with CO. The authors have assigned the

formation of the 2D Pd nano-objects to the slow kinetics of nucleation and growth when less reactive precursors were employed.

Zheng *et al.*,[135] employed the CO mediated growth of Pd ultrathin nanosheets with original optical and excellent electrocatalytic properties (Figure 6).

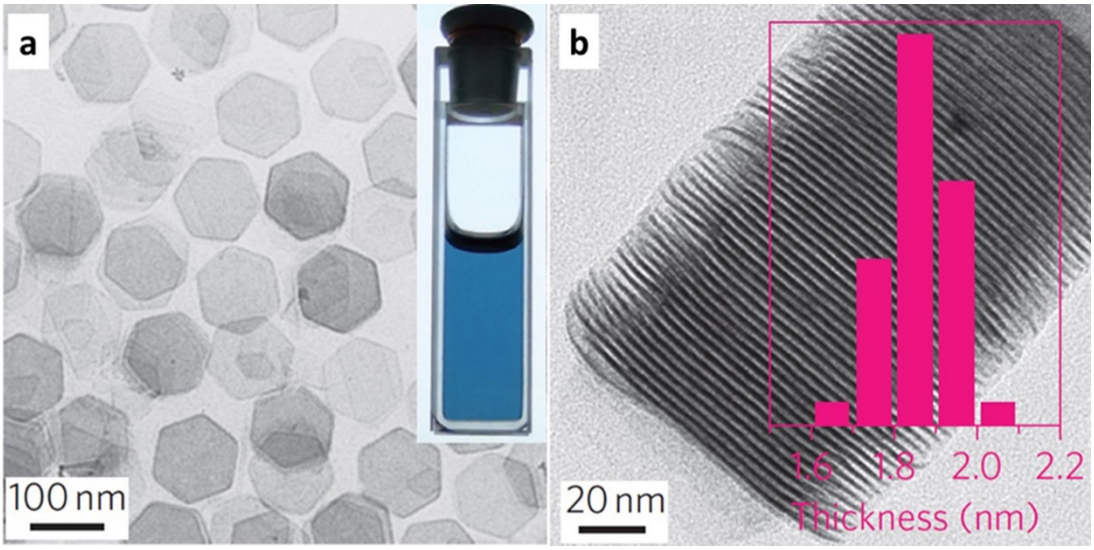

Figure 6. TEM images of (a) Pd nanosheets, inset: photograph of a dispersion of the nanosheets in ethanol; (b) an assembly of Pd nanosheets perpendicular to the TEM grid, and their thickness distribution. ***Adapted from ref. 135 with permission from Springer Nature Copyright 2011.***

[$Pd(acac)_2$] was reduced at low temperatures (r.t. to 100 °C) in the presence of PVP and ammonium halides in various organic solvents. Pd nanosheets of different sizes and excellent size distribution was achieved by adjusting the reaction conditions. Electrochemical CO stripping has revealed that 96% of the exposed nanosheet surface were Pd(111). The authors assigned the shape to the strong adsorption of CO on the {111} facets of the sheets, preventing growth along the <111> direction. Less efficient halide adsorption on the six halide-bound {100} facets allowed lateral growth. In a subsequent work by the same group, the anionic intermediate [$Pd_2(\mu$-

$CO)_2Cl_4]^{2-}$ was prepared by reaction of H_2PdCl_4 with CO. Ultrathin Pd nanosheets exposing {111} facets were obtained by simply adding water to a solution in DMF (DMF= dimethylformamide) of the intermediate $[Pd_2(\mu\text{-}CO)_2Cl_4]^{2-}$, in the absence of any organic capping agents. Control experiments have demonstrated that the CO ligands in $[Pd_2(\mu\text{-}CO)_2Cl_4]^{2-}$ reduce Pd(I) with concomitant CO oxidation to CO_2, and serve as capping agents for the formation of Pd nanosheets. The palladium nanosheets produced by this method did not contain any organic capping agent on their surface and exhibited improved catalytic and electrocatalytic properties compared to polymer capped Pd nanosheets.[136] In a recent work, Yang *et al*. suggested that $[Pd(acac)_2]$ reacted with acetic acid under CO to form a $[Pd_4(CO)_4(OAc)_4]$ intermediate, which adsorbs onto Pd {110} facets, directly leading to anisotropic growth along the <011> directions and the formation of hexagonal 2D Pd nano-objects.[137]

Interestingly, in a system that under CO gives rise to Pd nanosheets, and under H_2 forms Pd nanoaggregates, when both CO and H_2 ($CO:H_2$ = 1:4) are introduced, tetrahedra and tetrapods, both exposing {111} facets, are produced (Figure 7).[138] The formation of tetrahedra and tetrapods is attributed to the reduced CO adsorption energy on Pd{111} facets due to the presence of H_2. Based on experimental data and DFT calculations, the authors proposed a mechanism that involves the initial formation of NPs with a PdH_X phase, which is converted to Pd(0) upon exposure to air. Thus, in pure CO, the high CO coverage on Pd(111) prevents freshly reduced Pd atoms to deposit on {111} facets explaining why ultrathin nanosheets are formed. On the other hand, for PdH_x(111) surface, low CO coverage, allows Pd atoms to be directly deposited on PdH_x(111) surfaces, producing the 3D morphology.

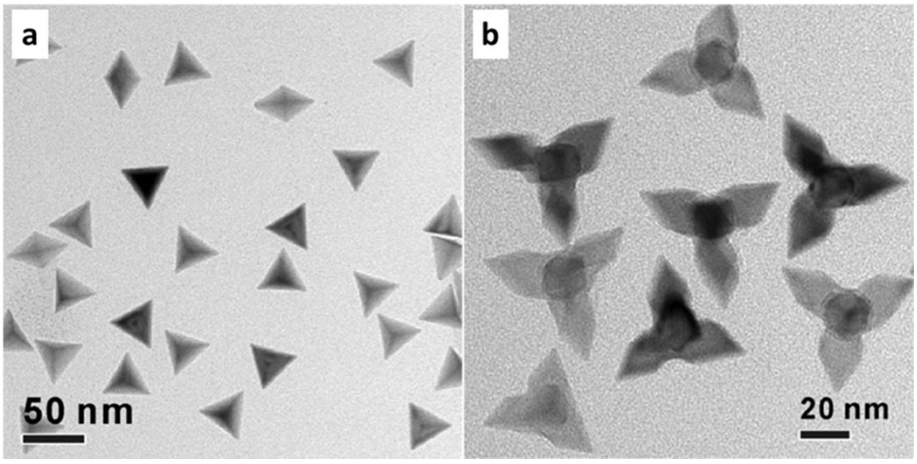

Figure 7. (a) Pd tetrahedral nanocrystals synthesized at 140 °C from $Pd(acac)_2$ in the presence of PVP and under 1:4 CO/H_2. (b) Pd tetrapods synthesized at 100 °C from $Pd(acac)_2$ in the presence of PVP and under 1:4 CO/H_2. ***Adapted from ref. 138 with permission from the American Chemical Society Copyright 2012.***

The simultaneous presence of CO and H_2 introduces additional possibilities in the panel of catalytic reactions that can take place on soluble metal species (hydroformylation) as well as on the NP surface (such as carbide formation, methanation, water gas shift, Fischer-Tropsch, etc.), the latter being possible especially with early transition metals that easily dissociate CO.

For instance, monodisperse iron carbide NPs that can be used as heating agents with high heating capacities were formed by direct reaction of CO and H_2 at 150 °C on preformed iron (0) NPs.[139] When combined with an appropriate catalyst they can magnetically activate various catalytic reactions.[139,140] Considering the mild reaction conditions under which carbidization takes place, similar to the ones employed in many syntheses of metal NPs, one can wonder whether similar reactions could not take place especially with early transition metals and in the presence of chemicals that can produce CO *in situ*. One example is described in the work of Meffre *et al*., in

which iron carbide NPs were produced by the reaction of $Fe(CO)_5$ with Fe(0) NPs at 150°C either under Ar or under H_2,[141] In another recent work, iron carbide nanoparticles were also produced in a continuous millifluidic system under N_2 from $Fe(CO)_5$ in the presence of oleylamine, albeit at higher temperatures (230 °C).[142]

4. Risks associated to the use of H_2 and CO and safety related best practices

Hydrogen is odorless and non-toxic, however, it is very flammable, requiring a small amount of energy to ignite. In fact, if leaking from a pipe at a high pressure, H_2 can self-ignite without the aid of an external energy source. It can also form an explosive mixture with the oxygen of the air. It has to be noted that gaseous hydrogen cannot be detected by the human senses, and its flame is also invisible. In fact, the range of hydrogen/air mixtures that will explode is wide: mixtures containing from as little as 4% v/v hydrogen, which is the Lower Explosive Limit (LEL), up to as much as 75% v/v, which is the Upper Explosive Limit (UEL), may propagate a flame. Hydrogen can be explosive at concentrations of 18.3%-59%.[143] However, it is important to note that an explosion cannot occur in a pure H_2 reservoir, since an oxidizer, such as oxygen, must be present in a concentration of at least 10% pure oxygen (or 41% air). The main risk is associated to any leaks that could fulfil the explosion/ignition conditions upon mixing with air. Therefore, hydrogen cylinders should be placed in a dedicated place outside the laboratory, connected with copper/stainless steel piping into the laboratory and secured to prevent tampering. Pipework should be regularly leak-checked to prevent large leaks of hydrogen. Fortunately, H_2 generators can very successfully replace gas cylinders. They generate gas on demand, as it is required by most of the laboratory set-ups for the synthesis of NPs. This means that they only store a minimal amount of gas, not enough to reach hydrogen's LEL (4.1% in air).

On the other hand, CO is also odorless, highly flammable, and, in contrast to H_2 which is non-toxic, it is highly toxic/poisonous and lethal if inhaled in not so high doses. The OSHA personal exposure limit (PEL) for CO is 50 parts per million (ppm). The NIOSH recommended immediately dangerous to life and health concentration (IDLH) for CO is 1,200 ppm. The IDLH is the concentration that could result in death or irreversible health effects, or prevent escape from the contaminated environment within 30 minutes. Carbon monoxide should be used in a fumehood and all valves, connections, regulators and fittings should be checked for leaks. A carbon monoxide detector should be in use while CO is flowing at the proximity of the experimental set-up and individual portable detectors should be worn by the users.

It is also important to note that the small amounts of gas reactants required and the relatively low pressures employed in the academic research for nanoparticle synthesis limit the risks of an accident, as the conditions for fire, explosion or intoxication are hardly met under adapted working conditions (appropriately installed gas cylinders and connections, fumehoods, adapted pressure vessels, pressure release devices).

To conclude, as for all chemicals, when working with H_2 or CO, it is essential to learn about their physico-chemical properties in order to know their behavior and, therefore, any possible associated risks. Appropriate practices have to be adopted and adapted to the working conditions and safety regulations of each laboratory. Prior to conducting any work with carbon monoxide, designated personnel must provide training, specific to the hazards involved in working with these substances, and detailed information on emergency procedures. Last but not least, safety equipment should always include detection systems and alarms as second line defense for possible leaks.

5. Conclusions

H_2 and CO are convenient reducing agents of intermediate strength, allowing the reduction of a large variety of metals by modulation of their reducing ability through the proper choice of reaction conditions. Depending on the reaction conditions they let behind little or no residues. This is especially true for H_2.

In some cases where H_2 and CO are used for the synthesis of nanoparticles, the reaction is not a not real reduction but a simple displacement of ligands from precursors in which the metal center is already reduced. Reductants or not, they can affect the outcome of the nanoparticle formation by various ways as exposed throughout this chapter.

After some decades of intensive research, the “black box” of nanoparticle synthesis is now starting to be less black thanks to the knowledge accumulated over the years. The recent development of cutting-edge characterization techniques combined to modeling have already significantly contributed, and they are expected to contribute even more in the near future to a better understanding of the possible reaction processes that lead to NP formation.[144] H_2 and CO have been used with many metals, under different reaction conditions and in the presence of very different capping agents, some of them being able to act as reducing agents, but only very few comparative studies which describe syntheses using the same reaction conditions where only the reducing agent is varied are available. This lack of data does not allow the evaluation of the real influence of the reducing agent on the nanoparticle structural characteristics. Another point worth to be noted is that these gases are most of the times used for reducing molecular metallic species in mixtures where other potential reducing agents are also present, which raises the question of their degree of participation in the reduction process. An answer to this question

requires an identification of the oxidized products, which is very rarely part of the usual investigation procedure in the domain of nanoparticle synthesis. In this respect, the use of new experimental and theoretical tools could give precious information. Thus, revisiting some of the most interesting examples is extremely important.

Last but not least, “analyzing” the inherent complexity of these reactions is a crucial step; however, “synthesizing” by combining the accumulated knowledge across several disciplines is equally essential towards a better understanding of the complex processes involved.

In this respect, when used as reducing agents for metal nanoparticle synthesis, H_2 and CO, are always supplied to the reaction medium in excess, large enough to be catalytically transformed. Most of the metals, either in their molecular form or in the solid state are active catalysts for a variety of reactions involving H_2 (hydrogenation), CO (carbonylation), or their mixture (water gas shift reaction, Fischer-Tropsch synthesis). From this point of view, the huge available knowledge on homogeneous and heterogeneous catalytic reactions, should be advantageously exploited in the domain of metal nanoparticle synthesis.

Acknowledgements

This work was partially supported by the EUR grant NanoX n° ANR-17-EURE-0009 in the framework of the "Programme des Investissements d’Avenir" through the project CaSh. The authors also thank ERC Advanced Grant (MONACAT 2015-694159) for financial support.

References

1. Y. Wang, J. He, C. Liu, W. H. Chong and H. Chen, *Angew. Chem. Int. Ed.*, 2015, **54**, 2022–2051.
2. M. Chen, B. Wu, J. Yang and N. Zheng, *Adv. Mater.*, 2012, **24**, 862–879.
3. S. Luidold and H. Antrekowitsch, *JOM*, 2007, **59**, 20–26.
4. D. Spreitzer and J. Schenk, *steel research int.*, 2019, **90**, 1900108.
5. L. Kvitek, R. Prucek, A. Panacek and J. Soukupova, in *Silver Nanoparticles - Health and Safety, Physicochemical Aspects of Metal Nanoparticle Preparation*, IntechOpen, 2019.
6. L. D. Rampino, F. F. Nord, *J. Chem. Soc.*, 1941, **63**, 2745-2749.
7. H. Hirai, Y. Nakao, N. Toshima, K. Adachi, Chem. Lett., 1976, 5, 905-910.
8. L. Hernandez and F. F. Nord, *J. Colloid Sci.*, 1948, **3**, 363–375.
9. W. P. Dunworth and F. F. Nord, *J. Am. Chem. Soc.*, 1950, **72**, 4197–4198.
10. G. S. McGrady and G. Guilera, *Chem. Soc. Rev.*, 2003, **32**, 383-392.
11. V. K. LaMer and R. H. Dinegar, *J. Am. Chem. Soc.*, 1950, **72**, 4847–4854.
12. K. Christmann, in *Encyclopedia of Interfacial Chemistry*, Elsevier, 2018, pp. 213–220.
13. Y. Lin and R. G. Finke, *J. Am. Chem. Soc.*, 1994, **116**, 8335–8353.
14. M. A. Watzky and R. G. Finke, *J. Am. Chem. Soc.*, 1997, **119**, 10382–10400.
15. S. Özkar and R. G. Finke, *J. Am. Chem. Soc.*, 2005, **127**, 4800–4808.
16. J. D. Aiken and R. G. Finke, *J. Am. Chem. Soc.*, 1999, **121**, 8803–8810.
17. J. Dupont and J. D. Scholten, *Chem. Soc. Rev.*, 2010, **39**, 1780-1804.
18. M. M. Giangregorio, M. Losurdo, G. V. Bianco, A. Operamolla, E. Dilonardo, A. Sacchetti, P. Capezzuto, F. Babudri and G. Bruno, *J. Phys. Chem. C*, 2011, **115**, 19520–19528.
19. T. S. Ahmadi, Z. L. Wang, T. C. Green, A. Henglein and M. A. El-Sayed, *Science*, 1996, **272**, 1924–1925.
20. A. R. Tao, S. Habas and P. Yang, *Small*, 2008, **4**, 310–325.
21. Y. Xia, Y. Xiong, B. Lim and S. E. Skrabalak, *Angew. Chem. Int. Ed.*, 2009, **48**, 60–103.
22. K. M. Bratlie, H. Lee, K. Komvopoulos, P. Yang and G. A. Somorjai, *Nano Lett.*, 2007, **7**, 3097–3101.
23. K. Zhou and Y. Li, *Angew. Chem. Int. Ed.*, 2012, **51**, 602–613.
24. J. M. Petroski, Z. L. Wang, T. C. Green and M. A. El-Sayed, *J. Phys. Chem. B* 1998, **102**, 3316-3320.
25. K. An and G. A. Somorjai, *ChemCatChem*, 2012, **4**, 1512–1524.
26. T. Teranishi, R. Kurita and M. Miyake, Journal of Inorganic and Organometallic Polymers, 2000, 10, 145-156.
27. X. Fu, Y. Wang, N. Wu, L. Gui and Y. Tang, *Langmuir*, 2002, **18**, 4619–4624.
28. H. Lee, S. E. Habas, S. Kweskin, D. Butcher, G. A. Somorjai and P. Yang, *Angew. Chem. Int. Ed.*, 2006, **45**, 7824–7828.
29. C. Salzemann and C. Petit, *Langmuir*, 2012, **28**, 4835–4841.
30. N. Aguilera-Porta, M. Calatayud, C. Salzemann and C. Petit, *J. Phys. Chem. C*, 2014, **118**, 9290–9298.
31. L.-M. Lacroix, C. Gatel, R. Arenal, C. Garcia, S. Lachaize, T. Blon, B. Warot-Fonrose, E. Snoeck, B. Chaudret and G. Viau, *Angew. Chem. Int. Ed.*, 2012, **51**, 4690–4694.

32. L. Peres, D. Yi, S. Bustos-Rodriguez, C. Marcelot, A. Pierrot, P.-F. Fazzini, I. Florea, R. Arenal, L.-M. Lacroix, B. Warot-Fonrose, T. Blon and K. Soulantica, *Nanoscale*, 2018, **10**, 22730–22736.
33. A. R. Poerwoprajitno, L. Gloag, S. Cheong, J. J. Gooding and R. D. Tilley, *Nanoscale*, 2019, **11**, 18995–19011.
34. C. Amiens, B. Chaudret, D. Ciuculescu-Pradines, V. Collière, K. Fajerwerg, P. Fau, M. Kahn, A. Maisonnat, K. Soulantica and K. Philippot, *New J. Chem.*, 2013, **37**, 3374.
35. C. Amiens, D. Ciuculescu-Pradines and K. Philippot, *Coord.Chem. Rev.*, 2016, **308**, 409–432.
36. A. Heuer-Jungermann, N. Feliu, I. Bakaimi, M. Hamaly, A. Alkilany, I. Chakraborty, A. Masood, M. F. Casula, A. Kostopoulou, E. Oh, K. Susumu, M. H. Stewart, I. L. Medintz, E. Stratakis, W. J. Parak, A. G. Kanaras, *Chem. Rev.*, 2019, **119**, 4819-4880.
37. K. Philippot and B. Chaudret, *Comptes Rendus Chimie*, 2003, **6**, 1019–1034.
38. B. Cormary, F. Dumestre, N. Liakakos, K. Soulantica and B. Chaudret, *Dalton Trans.*, 2013, **42**, 12546-12553.
39. D. Ciuculescu, C. Amiens, M. Respaud, A. Falqui, P. Lecante, R. E. Benfield, L. Jiang, K. Fauth and B. Chaudret, *Chem. Mater.*, 2007, **19**, 4624–4626.
40. J. S. Bradley, J. M. Millar, E. W. Hill, S. Behal, B. Chaudret and A. Duteil, *Faraday Disc.*, 1991, **92**, 255-268.
41. M. R. Axet, K. Philippot, B. Chaudret, M. Cabié, S. Giorgio and C. R. Henry, *Small*, 2011, **7**, 235–241.
42. E. Ramirez, L. Eradès, K. Philippot, P. Lecante and B. Chaudret, *Adv. Funct. Mater.*, 2007, **17**, 2219–2228.
43. E. Ramirez, S. Jansat, K. Philippot, P. Lecante, M. Gomez, A. M. Masdeu-Bultó and B. Chaudret, *J. Organomet.Chem.*, 2004, **689**, 4601–4610.
44. M. R. Axet, S. Castillón, C. Claver, K. Philippot, P. Lecante and B. Chaudret, *Eur. J. Inorg. Chem.*, 2008, **2008**, 3460–3466.
45. C. Barrière, K. Piettre, V. Latour, O. Margeat, C.-O. Turrin, B. Chaudret and P. Fau, *J. Mater. Chem.*, 2012, **22**, 2279–2285.
46. T. O. Ely, C. Amiens, B. Chaudret, E. Snoeck, M. Verelst, M. Respaud and J.-M. Broto, *Chem. Mater.*, 1999, **11**, 526–529.
47. F. Dumestre, B. Chaudret, C. Amiens, M. Respaud, P. Fejes, P. Renaud and P. Zurcher, *Angew. Chem. Int. Ed.*, 2003, **42**, 5213–5216.
48 T. Ayvalı, P. Lecante, P.-F. Fazzini, A. Gillet, K. Philippot and B. Chaudret, *Chem. Commun.*, 2014, **50**, 10809-10811.
49. M. Cokoja, H. Parala, M.-K. Schröter, A. Birkner, M. W. E. van den Berg, W. Grünert and R. A. Fischer, *Chem. Mater.*, 2006, **18**, 1634–1642.
50. M. Cokoja, H. Parala, M. K. Schröter, A. Birkner, M. W. E. van den Berg, K. V. Klementiev, W. Grünert and R. A. Fischer, *J. Mater. Chem.*, 2006, **16**, 2420–2428.
51. L. M. Martínez-Prieto and B. Chaudret, *Acc. Chem. Res.*, 2018, **51**, 376–384.
52. M. R. Axet and K. Philippot, *Chem. Rev.*, 2020, **120**, 1085–1145.
53. C. Pan, K. Pelzer, K. Philippot, B. Chaudret, F. Dassenoy, P. Lecante and M.-J. Casanove, *J. Am. Chem. Soc.*, 2001, **123**, 7584–7593.
54. P. Lara, K. Philippot and B. Chaudret, *ChemCatChem*, 2013, **5**, 28–45.
55. P. Lara, O. Rivada-Wheelaghan, S. Conejero, R. Poteau, K. Philippot and B. Chaudret, *Angew. Chem. Int. Ed.*, 2011, **50**, 12080–12084.
56. I. Favier, S. Massou, E. Teuma, K. Philippot, B. Chaudret and M. Gómez, *Chem. Commun.*, 2008, 3296-3298.

57. K. Pelzer, O. Vidoni, K. Philippot, B. Chaudret and V. Collière, *Adv. Funct. Mater.*, 2003, **13**, 118–126.
58. P. Lignier, R. Bellabarba, R. P. Tooze, Z. Su, P. Landon, H. Ménard and W. Zhou, *Cryst. Growth Des.*, 2012, **12**, 939–942.
59. F. Leng, I. C. Gerber, P. Lecante, W. Bacsa, J. Miller, J. R. Gallagher, S. Moldovan, M. Girleanu, M. R. Axet and P. Serp, *RSC Adv.*, 2016, **6**, 69135–69148.
60. E. Bresó-Femenia, C. Godard, C. Claver, B. Chaudret and S. Castillón, *Chem. Commun.*, 2015, **51**, 16342–16345.
61. T. Pery, K. Pelzer, G. Buntkowsky, K. Philippot, H.-H. Limbach and B. Chaudret, *ChemPhysChem*, 2005, **6**, 605–607.
62. R. González-Gómez, L. Cusinato, C. Bijani, Y. Coppel, P. Lecante, C. Amiens, I. del Rosal, K. Philippot and R. Poteau, *Nanoscale*, 2019, **11**, 9392–9409.
63. J. García-Antón, M. R. Axet, S. Jansat, K. Philippot, B. Chaudret, T. Pery, G. Buntkowsky and H.-H. Limbach, *Angew. Chem. Int. Ed.*, 2008, **47**, 2074–2078.
64. T. Gutmann, B. Walaszek, X. Yeping, M. Wächtler, I. del Rosal, A. Grünberg, R. Poteau, R. Axet, G. Lavigne, B. Chaudret, H.-H. Limbach and G. Buntkowsky, *J. Am. Chem. Soc.*, 2010, **132**, 11759–11767.
65. L. A. Truflandier, I. Del Rosal, B. Chaudret, R. Poteau and I. C. Gerber, *ChemPhysChem*, 2009, **10**, 2939–2942.
66. F. Schröder, D. Esken, M. Cokoja, M. W. E. van den Berg, O. I. Lebedev, G. Van Tendeloo, B. Walaszek, G. Buntkowsky, H.-H. Limbach, B. Chaudret and R. A. Fischer, *J. Am. Chem. Soc.*, 2008, **130**, 6119–6130.
67. D. González-Gálvez, P. Nolis, K. Philippot, B. Chaudret and P. W. N. M. van Leeuwen, *ACS Catal.*, 2012, **2**, 317–321.
68. Y. Min, H. Nasrallah, D. Poinsot, P. Lecante, Y. Tison, P. Roblin, A. Falqui, R. Poteau, M. R. Axet and P. Serp, *Chem. Mater.*, 2020, 14, 2365-2378.
69. G. Pieters, C. Taglang, E. Bonnefille, T. Gutmann, C. Puente, J.-C. Berthet, C. Dugave, B. Chaudret and B. Rousseau, *Angew. Chem. Int. Ed.*, 2014, **53**, 230–234.
70. C. Taglang, L. M. Martínez-Prieto, I. del Rosal, L. Maron, R. Poteau, K. Philippot, B. Chaudret, S. Perato, A. Sam Lone, C. Puente, C. Dugave, B. Rousseau and G. Pieters, *Angew. Chem. Int. Ed.*, 2015, **54**, 10474–10477.
71. L. Cusinato, L. M. Martínez-Prieto, B. Chaudret, I. del Rosal and R. Poteau, *Nanoscale*, 2016, **8**, 10974–10992.
72. L. M. Martínez-Prieto, S. Carenco, C. H. Wu, E. Bonnefille, S. Axnanda, Z. Liu, P. F. Fazzini, K. Philippot, M. Salmeron and B. Chaudret, *ACS Catal.*, 2014, **4**, 3160–3168.
73. F. Leng, I. C. Gerber, P. Lecante, S. Moldovan, M. Girleanu, M. R. Axet and P. Serp, *ACS Catal.*, 2016, **6**, 6018–6024.
74. I. M. L. Billas, A. Chatelain and W. A. de Heer, *Science*, 1994, **265**, 1682–1684.
75. M. Respaud, J. M. Broto, H. Rakoto, A. R. Fert, L. Thomas, B. Barbara, M. Verelst, E. Snoeck, P. Lecante, A. Mosset, J. Osuna, T. O. Ely, C. Amiens and B. Chaudret, *Phys. Rev. B*, 1998, **57**, 2925–2935.
76. J. Osuna, D. de Caro, C. Amiens, B. Chaudret, E. Snoeck, M. Respaud, J.-M. Broto and A. Fert, *J. Phys. Chem.*, 1996, **100**, 14571–14574.
77. N. Cordente, C. Amiens, B. Chaudret, M. Respaud, F. Senocq and M.-J. Casanove, *Journal of Applied Physics*, 2003, **94**, 6358–6365.
78. F. Dumestre, B. Chaudret, C. Amiens, M.-C. Fromen, M. J. Casanove, P. Renaud, P. Zurcher, *Angew. Chem. Int. Ed.* 2002, **41**, 4286-4289.

79. D. Ciuculescu, F. Dumestre, M. Comesaña-Hermo, B. Chaudret, M. Spasova, M. Farle and C. Amiens, *Chem. Mater.*, 2009, **21**, 3987–3995.
80. B. Cormary, T. Li, N. Liakakos, L. Peres, P.-F. Fazzini, T. Blon, M. Respaud, A. J. Kropf, B. Chaudret, J. T. Miller, E. A. Mader and K. Soulantica, *J. Am. Chem. Soc.*, 2016, **138**, 8422–8431.
81. F. Dumestre, B. Chaudret, C. Amiens, P. Renaud, P. Fejes, *Science*, 2004, **303**, 821–823.
82. F. Wetz, K. Soulantica, M. Respaud, A. Falqui and B. Chaudret, *Mat. Sci. Eng. C*, 2007, **27**, 1162-1166.
83. M. He, L. Protesescu, R. Caputo, F. Krumeich and M. V. Kovalenko, *Chem. Mater.*, 2015, **27**, 635–647.
84. O. Margeat, F. Dumestre, C. Amiens, B. Chaudret, P. Lecante and M. Respaud, *Progress in Solid State Chemistry*, 2005, **33**, 71–79.
85. L.-M. Lacroix, S. Lachaize, A. Falqui, M. Respaud and B. Chaudret, *J. Am. Chem. Soc.*, 2009, **131**, 549–557.
86. N. Liakakos, B. Cormary, X. Li, P. Lecante, M. Respaud, L. Maron, A. Falqui, A. Genovese, L. Vendier, S. Koïnis, B. Chaudret and K. Soulantica, *J. Am. Chem. Soc.*, 2012, **134**, 17922–17931.
87. N. Liakakos, C. Gatel, T. Blon, T. Altantzis, S. Lentijo-Mozo, C. Garcia-Marcelot, L.-M. Lacroix, M. Respaud, S. Bals, G. Van Tendeloo and K. Soulantica, *Nano Lett.*, 2014, **14**, 2747–2754.
88. C. Garnero, M. Lepesant, C. Garcia-Marcelot, Y. Shin, C. Meny, P. Farger, B. Warot-Fonrose, R. Arenal, G. Viau, K. Soulantica, P. Fau, P. Poveda, L.-M. Lacroix and B. Chaudret, *Nano Lett.*, 2019, **19**, 1379–1386.
89. S. Mourdikoudis, V. Collière, C. Amiens, P. Fau and M. L. Kahn, *Langmuir*, 2013, **29**, 13491–13501.
90. G. L. Drisko, C. Gatel, P.-F. Fazzini, A. Ibarra, S. Mourdikoudis, V. Bley, K. Fajerwerg, P. Fau and M. Kahn, *Nano Lett.*, 2018, **18**, 1733–1738.
91. X. Liang, N. Liu, H. Qiu, C. Zhang, D. Mei and B. Chen, *Phys. Chem. Chem. Phys.*, 2017, **19**, 26718–26727.
92. X. Wang, N. Liu, C. Dai, R. Xu, B. Wu, G. Yu and B. Chen, *J. Phys. Chem. C*, 2020, **124**, 2160–2170.
93. A. P. LaGrow, B. Ingham, S. Cheong, G. V. M. Williams, C. Dotzler, M. F. Toney, D. A. Jefferson, E. C. Corbos, P. T. Bishop, J. Cookson and R. D. Tilley, *J. Am. Chem. Soc.*, 2012, **134**, 855–858.
94. A. P. LaGrow, S. Cheong, J. Watt, B. Ingham, M. F. Toney, D. A. Jefferson and R. D. Tilley, *Adv. Mater.*, 2013, **25**, 1552–1556.
95. A. R. Poerwoprajitno, L. Gloag, J. Watt, S. Cychy, S. Cheong, P. V. Kumar, T. M. Benedetti, C. Deng, K.-H. Wu, C. E. Marjo, D. L. Huber, M. Muhler, J. J. Gooding, W. Schuhmann, D.-W. Wang and R. D. Tilley, *Angew. Chem. Int. Ed.*, 2020, 59, 15487-15491.
96. Y. Bing, H. Liu, L. Zhang, D. Ghosh and J. Zhang, *Chem. Soc. Rev.*, 2010, **39**, 2184-2202.
97. R. Xie, Y. Pan and H. Gu, *RSC Adv.*, 2015, **5**, 16497–16500.
98. J. Mao, W. Chen, D. He, J. Wan, J. Pei, J. Dong, Y. Wang, P. An, Z. Jin, W. Xing, H. Tang, Z. Zhuang, X. Liang, Y. Huang, G. Zhou, L. Wang, D. Wang and Y. Li, *Sci. Adv.*, 2017, **3**, e1603068.
99. R. K. Ramamoorthy, A. Viola, B. Grindi, J. Peron, C. Gatel, M. Hytch, R. Arenal, L. Sicard, M. Giraud, J.-Y. Piquemal and G. Viau, *Nano Lett.*, 2019, **19**, 9160–9169.
100 J. Wu, Y. Huang, W. Ye and Y. Li, *Adv. Sci.*, 2017, **4**, 1700194.

101. R. H. Crabtree, in *The Organometallic Chemistry of the Transition Metals*, John Wiley & Sons, Inc., Hoboken, NJ, USA, 2005, pp. 87–124.
102. S. S. Sung and R. Hoffmann, *J. Am. Chem. Soc.*, 1985, **107**, 578–584.
103. S. Y. Hwang, M. Zhang, C. Zhang, B. Ma, J. Zheng and Z. Peng, *Chem. Commun.*, 2014, **50**, 14013–14016.
104. J. Rabo, *Journal of Catalysis*, 1978, **53**, 295–311.
105. G. P. Valença and E. S. Gonçalves, in *Studies in Surface Science and Catalysis*, Elsevier, 2001, vol. 133, pp. 399–407.
106. A. Duteil, R. Queau, B. Chaudret, R. Mazel, C. Roucau and J. S. Bradley, *Chem. Mater.*, 1993, **5**, 341–347.
107. C. Amiens, D. de Caro, B. Chaudret, J. S. Bradley, R. Mazel and C. Roucau, *J. Am. Chem. Soc.*, 1993, **115**, 11638–11639.
108. S. Ishi and Y. Ohno, *Surf. Sci.*, 1985, **161**, 349-372.
109. T. M. Duncan, K. W. Zilm, D. M. Hamilton and T. W. Root, *J. Phys. Chem.* 1989, **93**, 2583-2590.
110. F. Novio, K. Philippot and B. Chaudret, *Catal Lett*, 2010, **140**, 1–7.
111. F. Novio, D. Monahan, Y. Coppel, G. Antorrena, P. Lecante, K. Philippot and B. Chaudret, *Chem. Eur. J.*, 2014, **20**, 1287–1297.
112. J. S. Bradley, E. W. Hill, B. Chaudret and A. Duteil, *Langmuir*, 1995, **11**, 693–695.
113. X. Cheng, Z. Shi, N. Glass, L. Zhang, J. Zhang, D. Song, Z.-S. Liu, H. Wang and J. Shen, *J. Power Sources*, 2007, **165**, 739–756.
114. Y. Yu, Z. Luo, Y. Yu, J. Y. Lee and J. Xie, *ACS Nano*, 2012, **6**, 7920–7927.
115. T. Chen and J. Xie, *Chem. Rec.*, 2016, **16**, 1761–1771.
116. N. Goswami, Q. Yao, T. Chen and J. Xie, *Coord. Chem. Rev.* 2016, **329**, 1–15.
117. V. Latour, A. Maisonnat, Y. Coppel, V. Collière, P. Fau and B. Chaudret, *Chem. Commun.*, 2010, **46**, 2683-2685.
118. P.-J. Debouttière, Y. Coppel, P. Behra, B. Chaudret and K. Fajerwerg, *Gold Bull*, 2013, **46**, 291–298.
119. J. Pal and T. Pal, *Nanoscale*, 2015, **7**, 14159–14190.
120. J. Wu, L. Qi, H. You, A. Gross, J. Li and H. Yang, *J. Am. Chem. Soc.*, 2012, **134**, 11880–11883.
121. F. Nosheen, N. Wasfi, S. Aslam, T. Anwar, S. Hussain, N. Hussain, S. N. Shah, N. Shaheen, A. Ashraf, Y. Zhu, H. Wang, J. Ma, Z. Zhang and W. Hu, *Nanoscale*, 2020, **12**, 4219–4237.
122. J. W. Hong, Y. Kim, D. H. Wi, S. Lee, S.-U. Lee, Y. W. Lee, S.-I. Choi and S. W. Han, *Angew. Chem. Int. Ed.*, 2016, **55**, 2753–2758.
123. L. Zhao, C. Xu, H. Su, J. Liang, S. Lin, L. Gu, X. Wang, M. Chen and N. Zheng, *Adv. Sci.*, 2015, **2**, 1500100.
124. C. Wang, H. Daimon, T. Onodera, T. Koda and S. Sun, *Angew. Chem. Int. Ed.*, 2008, **47**, 3588 –3591
125. S. I. Lim, I. Ojea-Jiménez, M. Varon, E. Casals, J. Arbiol and V. Puntes, *Nano Lett.*, 2010, **10**, 964–973.
126. J. Zhang and J. Fang, *J. Am. Chem. Soc.*, 2009, **131**, 18543–18547.
127. J. Wu, A. Gross and H. Yang, *Nano Lett.*, 2011, **11**, 798–802.
128. Y. Kang, X. Ye and C. B. Murray, *Angewandte Chemie*, 2010, **122**, 6292–6295.
129. B. Wu, N. Zheng and G. Fu, *Chem. Commun.*, 2011, **47**, 1039–1041.
130. M. Xie, Z. Lyu, R. Chen and Y. Xia, *Chem. Eur. J.*, 2020, DOI: 10.1002/chem.202003202.

131. Y. Wang, Z. Sun, A. Kumbhar, Z. Luo, C. Wang, J. Zhang, N. Porter, C. Xu, K. Sun, B. Martens and J. Fang, *Chem. Commun.*, 2013, **49**, 3955-3957.
132. Y. Chen, Z. Fan, Z. Zhang, W. Niu, C. Li, N. Yang, B. Chen and H. Zhang, *Chem. Rev.*, 2018, **118**, 6409–6455.
133. U. Schlotterbeck, C. Aymonier, R. Thomann, H. Hofmeister, M. Tromp, W. Richtering and S. Mecking, *Adv. Funct. Mater.*, 2004, **14**, 999–1004.
134. P. F. Siril, L. Ramos, P. Beaunier, P. Archirel, A. Etcheberry and H. Remita, *Chem. Mater.*, 2009, **21**, 5170–5175.
135. X. Huang, S. Tang, X. Mu, Y. Dai, G. Chen, Z. Zhou, F. Ruan, Z. Yang and N. Zheng, *Nature Nanotech*, 2011, **6**, 28–32.
136. H. Li, G. Chen, H. Yang, X. Wang, J. Liang, P. Liu, M. Chen and N. Zheng, *Angew. Chem. Int. Ed.*, 2013, **52**, 8368–8372.
137. X. Yin, X. Liu, Y.-T. Pan, K. A. Walsh and H. Yang, *Nano Lett.*, 2014, **14**, 7188–7194.
138. Y. Dai, X. Mu, Y. Tan, K. Lin, Z. Yang, N. Zheng and G. Fu, *J. Am. Chem. Soc.*, 2012, **134**, 7073–7080.
139. A. Bordet, L.-M. Lacroix, P.-F. Fazzini, J. Carrey, K. Soulantica and B. Chaudret, *Angew. Chem. Int. Ed.*, 2016, **55**, 15894–15898.
140. J. M. Asensio, A. B. Miguel, P. Fazzini, P. W. N. M. van Leeuwen and B. Chaudret, *Angew. Chem. Int. Ed.*, 2019, **58**, 11306–11310.
141. A. Meffre, B. Mehdaoui, V. Kelsen, P. F. Fazzini, J. Carrey, S. Lachaize, M. Respaud and B. Chaudret, *Nano Lett.*, 2012, **12**, 4722–4728.
142. K. Loizou, S. Mourdikoudis, A. Sergides, M. O. Besenhard, C. Sarafidis, K. Higashimine, O. Kalogirou, S. Maenosono, N. T. K. Thanh and A. Gavriilidis, *ACS Appl. Mater. Interfaces*, 2020, **12**, 28520–28531.
143. P. Ruiz, *Hydrogen: applications and safety considerations*, Matgas 2000 AIE, Bellaterra, Barcelona, 2015
144. S. Mourdikoudis, R. M. Pallares and N. T. K. Thanh, *Nanoscale*, 2018, **10**, 12871–12934.